Chemical Science

ROYAL SOCIETY OF CHEMISTRY

EDGE ARTICLE

View Article Online
View Journal | View Issue

Cite this: *Chem. Sci.*, 2021, **12**, 11894

All publication charges for this article have been paid for by the Royal Society of Chemistry

Contributions to cytochrome *c* inner- and outer-sphere reorganization energy†

Samir Chattopadhyay,[a] Manjistha Mukherjee,[a] Banu Kandemir,[b] Sarah E. J. Bowman,[b] Kara L. Bren *[b] and Abhishek Dey *[a]

Received 27th May 2021
Accepted 5th August 2021

DOI: 10.1039/d1sc02865k

rsc.li/chemical-science

Cytochromes *c* are small water-soluble proteins that catalyze electron transfer in metabolism and energy conversion processes. *Hydrogenobacter thermophilus* cytochrome c_{552} presents a curious case in displaying fluxionality of its heme axial methionine ligand; this behavior is altered by single point mutation of the Q64 residue to N64 or V64, which fixes the ligand in a single configuration. The reorganization energy (λ) of these cytochrome c_{552} variants is experimentally determined using a combination of rotating disc electrochemistry, chronoamperometry and cyclic voltammetry. The differences between the λ determined from these complementary techniques helps to deconvolute the contribution of the active site and its immediate environment to the overall λ (λ_{Total}). The experimentally determined λ values in conjunction with DFT calculations indicate that the differences in λ among the protein variants are mainly due to the differences in contributions from the protein environment and not just inner-sphere λ. DFT calculations indicate that the position of residue 64, responsible for the orientation of the axial methionine, determines the geometric relaxation of the redox active molecular orbital (RAMO). The orientation of the RAMO with respect to the heme is key to determining electron transfer coupling (H_{AB}) which results in higher ET rates in the wild-type protein relative to the Q64V mutant despite a 150 mV higher λ_{Total} in the former.

Introduction

Electron transfer (ET) reactions play important roles in diverse biological processes like photosynthesis and respiration and are key to energy transduction processes in all living organisms.[1–7] In systems for artificial photosynthesis, ET plays an equally important fundamental role and thus factors that control ET rates also are of interest to chemists and physicists.[8,9] The kinetics of ET (k_{ET}) in biological systems can be best understood by the help of the semi-classical Marcus equation depicted as follows:[10,11]

$$k_{ET} = \frac{4\Pi^2 {H_{AB}}^2}{h\sqrt{4\Pi\lambda k_B T}} \exp\left[-\left(\Delta G^0 + \lambda\right)^2 \Big/ 4\lambda k_B T\right] \quad (1)$$

H_{AB} denotes the electronic coupling between the donor and acceptor, $-\Delta G^0$ is the driving force for ET and λ denotes the total reorganization energy (λ_{Total}).[12,13] The value of λ_{Total} is the sum of two components: $\lambda_{Total} = \lambda_{IS} + \lambda_{OS}$.[12,14,15] The inner-sphere contribution (λ_{IS}) is the energy related to the change in geometry of the active site during oxidation and reduction.[14,16–18] It is mainly determined from the differences in equilibrium coordination geometry between the oxidized and reduced forms of the redox species involved in ET.[19] In the case of ET proteins containing heme cofactors, the charge/hole created due to the redox event efficiently delocalizes over the porphyrin ring, which contributes to a low λ_{IS} value.[15] The λ_{OS} for small molecules is the energy corresponding to the reorganization of the outer-sphere solvent shell adjacent to the redox species.[14] For redox sites in metalloproteins, λ_{OS} describes changes in the polypeptide environment of the redox site (represented here as λ_P) as well as solvent rearrangement (represented here as λ_{Solv}) such that $\lambda_{OS} = \lambda_P + \lambda_{Solv}$.[17,19] Typically, in electron transfer proteins, nature lowers λ_{OS} by harboring the redox site within a hydrophobic protein interior, excluding solvent, yielding a low λ_{Solv}.[17] Although λ is a critical parameter in determining ET rates, its reliable measurement is a long-standing challenge to chemists and biochemists.[18,20]

Direct protein electrochemistry can serve as an experimental tool to evaluate the λ of redox-active species.[21,22] In protein electrochemistry the desired protein can be immobilized on a self-assembled monolayer (SAM) modified Au electrode and the ET rate from the electrode to the protein can be determined as a function of temperature.[23,24] The temperature-dependent ET rate yields the λ using Arrhenius analysis.[15,25,26] The λ of cyt *c* from horse heart was previously determined electrochemically

[a]*School of Chemical Sciences, Indian Association for the Cultivation of Science, 2A Raja SC Mullick Road, Kolkata, WB, 700032, India. E-mail: icad@iacs.res.in*

[b]*Department of Chemistry, University of Rochester, Rochester, NY, 14627-0216, USA. E-mail: bren@chem.rochester.edu*

† Electronic supplementary information (ESI) available. See DOI: 10.1039/d1sc02865k

by Bowden and Tarlov *et al.* by immobilizing the protein on a 16-mercaptohexadecanoic acid (16-MHDA) modified Au electrode.[23] The λ can also be determined using the self-exchange ET rates of proteins and can be estimated from theoretical calculations.[20,27–31] The current electrochemical approach used in the determination of λ utilizes static electrochemical methods where mass transfer effects may affect the rates.[22,23]

Among the different members of the cytochrome *c* family, *Hydrogenobacter thermophilus* cytochrome c_{552} (HtWT) (Fig. 1A) is notable for the fluxionality of its axial methionine (Met) side chain ligated to the heme iron.[32,33] Furthermore, NMR analysis of site-directed mutants of HtWT shows that replacing glutamine, the 64th residue, (Q64) with valine (HtQ64V) or asparagine (HtQ64N) restricts the orientation of the axial methionine, resulting in *R*-configured methionine in HtQ64V whereas HtQ64N has the methionine in the *S* configuration (Fig. 1B).[32,34] These different configurations correspond to different orientations of the axial Met S p(π) orbitals relative to the heme plane and result in different orientations of the orbital hole on the oxidized heme, with proposed consequences for ET function.[35] This makes Ht cyt *c* and its variants a valuable model system for the study of the effects of heme axial Met orientation on electronic structure and ET function, including how the heme active site structure influences λ of electron transfer.[36]

In this manuscript, we apply three distinct electrochemical techniques to determine λ for HtWT, HtQ64N, and HtQ64V. Our general approach is to measure ET rates as a function of temperature and obtain values for λ from Arrhenius analysis. Furthermore, manipulation of reaction conditions and comparison to computational data yields insights into contributions of polypeptide and solvent to λ. First, we use rotating disc electrochemistry (RDE) to determine the temperature dependence of the second-order ET rate and the corresponding reorganization energies. These experiments are performed under conditions where the proteins are freely diffusing, allowing the measurements of all the factors which can contribute to the λ. Hence, we refer to this as λ_{Total}. This dynamic electrochemical technique for the determination of the λ_{Total} is validated using two well-characterized redox systems, an inorganic complex ($[Fe(CN)_6]^{3-/4-}$) and an electron transfer protein (bovine heart cyt *c*, b-cyt *c*). For the other two approaches, the proteins were immobilized on a 6-mercaptohexanoic acid SAM-modified Au electrode. One of these ET rate measurements used a chronoamperometric technique and the other used cyclic voltammetry (CV) analyzed according to Laviron's formalism. Corresponding reorganization energies measured with the help of these approaches are denoted as λ_{CA} and λ_{LV} hereafter, respectively. Note that, in spite of the immobilization of the proteins on the functionalized electrodes, the contribution of the solvent component cannot be completely nullified when the reorganization energies are measured using the above-mentioned approaches. Thus both λ_{CA} and λ_{LV} includes the contribution of λ_{IS}, λ_P and partly $\lambda_{solvent}$. However, DFT calculations performed on these mutants estimate the λ_{IS} and the contribution of the nearby residues to the λ_{OS}, *i.e.*, λ_P, but does not include any contribution from $\lambda_{solvent}$. The differences in the computed reorganization energies (λ_{cal}) among the protein variants obtained from DFT calculations are in good agreement with the differences in the reorganization energies obtained experimentally, suggesting that these differences in reorganization energy between the mutants originate from changes in the active site its immediate vicinity (*i.e.*, λ_{IS} and λ_P). These calculations help to elucidate the contribution of the axial methionine orientation and its interaction with a second-sphere residue in determining reorganization energy and H_{AB}, key factors determining rates in biological ET.

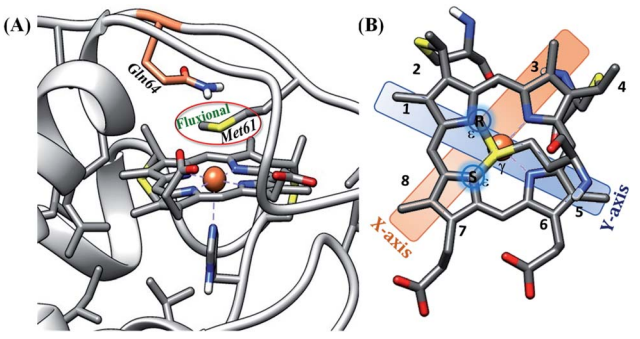

Fig. 1 (A) Active site structure of cytochrome c_{552} (PDB ID: 1AYG) (HtWT, as mentioned in our study). Here, Q64 is presented in orange. (B) The heme *c* cofactor of HtWT covalently attached to the polypeptide *via* two thioether bonds. Two axial Met orientations are overlayed, one with the δS–εC bond along the *X*-axis (plane containing peripheral $^3CH_3$–$^8CH_3$) denoted as Met in *S* configuration and the other with the δS–εC bond along the *Y* axis (plane containing peripheral $^1CH_3$–$^5CH_3$) known as Met in *R* configuration.

Experimental details

All reagents were of the highest grade commercially available and were used without further purification. Bovine heart cytochrome *c*, 6-mercaptohexanoic acid, and potassium hexafluorophosphate (KPF_6) were purchased from Sigma-Aldrich. Disodium hydrogen phosphate dihydrate ($NaH_2PO_4 \cdot 2H_2O$), potassium hexacyanoferrate(III) ($K_3[Fe(CN)_6]$), and absolute ethanol were purchased from Merck.

Instrumentation

All electrochemical experiments were performed using a CH instruments (CHI720D electrochemical analyzer) bipotentiostat. Aqueous Ag/AgCl (saturated KCl) and platinum were used as reference and counter electrodes, respectively, throughout the experiments. Teflon® plate material evaluating cells (PTM, ALS Japan) used in our study were purchased from CH instruments. The rotating ring disc electrochemical setup (RRDE) from Pine research instrumentation (E6 series change disc tips with the AFE6M rotor) was used to obtain the RDE data.

Protein expression and purification

Expression and purification of the proteins were done as described in the literature.[32,34]

Construction of the electrodes

Formation of self-assembled monolayer (SAM). Au wafers were cleaned electrochemically by sweeping several times between 1.6 V and −0.3 V *versus* aqueous Ag/AgCl (saturated KCl) in 0.5 M H_2SO_4. Au discs (surface area is 0.19625 cm^2) were polished in alumina (size: 1, 0.3, 0.05 μm) followed by electrochemical cleaning using the same procedure as cleaning of Au wafers. SAM solutions were prepared using 1 mM 6-mercaptohexanoic acid in absolute ethanol. Freshly cleaned Au wafers and discs were rinsed with Milli-Q water and ethanol, dried in N_2 and immediately immersed in SAM solution for 48 hours.

Electrostatic attachment of proteins onto the self-assembled monolayer (SAM). Au wafers were taken out of the SAM solution before each experiment and washed with ethanol and water and dried under a stream of N_2 gas. Au wafers were inserted in a plate material evaluating cell (ALS, Japan). Cytochrome *c* variants were adsorbed on the SAM-modified Au electrode by exposure of a 40 μM protein solution in 100 mM pH 7.3 sodium phosphate buffer (having 4 mM KPF_6 as the supporting electrolyte) at 4 °C for 4 h[23] The increase in the electrolyte concentration in the buffer can result in the complete desorption of the adsorbed Cyt *c* layer.

Electrochemical experiments

Au wafers, inserted in a plate material evaluating cell (the effective area for electrochemical studies is 0.45 cm^2 once the Au wafer was inserted in plate material evaluating cell) were then washed with Milli-Q water thrice and dried under a stream of N_2 gas. CV was performed with varying scan rates in 100 mM pH 7.3 sodium phosphate buffer containing 4 mM KPF_6 using aqueous Ag/AgCl (saturated KCl) and platinum electrodes as reference and counter electrodes, respectively, at different temperatures noted in the results section.

Chronoamperometric technique. Chronoamperometry was performed by taking the $E_{1/2,}$ measured by CV, of the corresponding protein, electrostatically attached to the modified Au electrodes, as an initial value and $E_{1/2}$ −50 mV ($E_{1/2}$ + 50 mV is also shown in the ESI†) as the final value using aqueous Ag/AgCl (saturated KCl) and Pt as reference and counter electrode, respectively. The capacitive current decays much faster than the corresponding faradaic current decay.[37] During our study we have constrained the evaluation of ET rate in such range of time scale (5 times greater than the charging current decay) in which we avoid the charging current effects on the faradaic current decay.[38] Values for apparent heterogeneous ET rate (k_{app}) were determined from the slope of the linear semilogarithmic plot of ln(i) *versus* t.[39] Here, a −50 mV potential step, ($\eta = E - E'$), *i.e.*, a lower driving force of ET, was applied relative to the formal potential of the cyt *c* attached to 6-mercaptohexanoic acid modified Au electrode and the corresponding cathodic decay constants were determined. The apparent ET rates of bovine heart cyt *c* (b-cyt *c*), HtWT and two mutants (HtQ64V, HtQ64N) were determined from the chronoamperometry analysis.

Rotating disc electrochemical technique. Rotating disc electrochemistry was performed using a 6-mercaptohexanoic acid SAM modified Au electrode, mounted on platinum ring disc assembly (Pine Instruments, USA) with corresponding protein dissolved in 100 mM pH 6 sodium phosphate buffer containing 150 mM KPF_6 under an argon atmosphere and at different temperatures as mentioned in the results section. The high concentration of electrolyte was used to prevent any attachment of the positively charged protein to the carboxyl-terminated alkyl thiol SAM-modified electrodes.

Surface coverage measurement

Surface coverage determinations of a 6-mercaptohexanoic acid monolayer on the modified Au electrode were done by reductive desorption method.[40,41] The reductive desorption of the monolayer was done in an ethanolic solution of 0.5 M KOH under an argon atmosphere using aqueous Ag/AgCl (saturated KCl) and a platinum electrode as reference and counter electrode, respectively, by scanning from −0.2 V to −1.2 V at a 20 mV s^{-1} scan rate. The area under the cathodic peak gives the surface coverage of the monolayer on the Au disc.

Density functional theory (DFT) calculations

The coordinates for HtWT were obtained from the protein data bank (PDB ID of HtWT is 1AYG).[42] Peptide truncation was achieved by substituting –C(=O)NH groups with –C(=O)H; these H were frozen in all calculations (Fig. 14). The model includes the proximal peptide loop including the two cysteine residues that are covalently attached to the heme and the axial His (residues 12–16). On the distal side of the heme, the peptide loop including the axial ligand M61 to the Q64 residue (which is being mutated) is included. It was further ensured that no hydrogen bonding interaction to the Q64 residue was excluded in this model. The structures of Q64V and Q64N mutants were obtained by replacing the glutamine residue (64th position, using *P. aeruginosa* cyt c_{551} numbering) in HtWT with valine and asparagine, respectively, and changing the orientation of the methionine according to the reported literature (Fig. 1B).[32,34] In the case of HtWT, two sets of structures with axial Met in both *R* and *S* configurations for both oxidized and reduced heme were optimized. In the case of HtQ64V and HtQ64N, the structures were optimized with the axial Met in the *R* and *S* configuration, respectively. The axial Met orientation was kept constant during the calculations of oxidized and reduced state geometry in each of the structures. The geometries of HtWT, HtQ64V and HtQ64N were optimized using unrestricted BP86 and B3LYP functional with gradient correction with the help of Gaussian 03 version (g03) in the gas phase.[43] The 6-31G(d) basis set was used for optimization of all of the atoms. Frequency calculations were performed on the optimized geometry to confirm that the minimum energy was obtained and the absence of any imaginary modes in these models. The 6-311+G(d) basis set was used on all of the atoms to determine the final energy of the models.[44,45] The λ values and redox potential values were obtained as the summation of the reorganization energy of the oxidized complex (λ_{ox}) and that of the reduced complex (λ_{red}).[14,15,46–50] The value of λ_{ox} can be calculated from the difference in energy between the Fe(III) at its optimized geometry and at the optimized geometry of Fe(III) within the Fe(II)

structure. The difference in energy between the optimized Fe(II) structure and Fe(II) in the optimal structure for Fe(III) gives the value of λ_{red}. The spin density distributions were determined using the cubegen utility of Gaussian 03 with an isovalue of 0.0004 and the LUMOs were created using the Chemissian software with an isovalue of 0.035.

Results and analysis

Electron transfer kinetics from rotating disc electrochemistry

Rotating Disc Electrochemistry (RDE) is used to determine the λ for redox active species in solution. To establish the validity of the method first RDE is used to determine the λ of well-known redox species like $[Fe(CN)_6]^{4-/3-}$ and bovine cyt *c* (b-cyt c) and then we proceed to evaluate the λ for Ht cyt *c*.

(A) $K_3[Fe(CN)_6]$. Cyclic voltammetry (Fig. S1†) and rotating RDE (Fig. S2†) of 1 mM $[Fe(CN)_6]^{3-}$ in 100 mM pH 7 sodium phosphate buffer containing 100 mM KPF_6 are performed at 283 K, 288 K, 293 K, and 298 K using freshly cleaned Au disc working electrodes. During RDE, the current at the working electrode increases with increasing rate of rotation following the Koutecký–Levich equation (K–L equation):

$$i^{-1} = i_K(E)^{-1} + i_L{}^{-1} \quad (2)$$

where $i_K(E)$ is the potential-dependent kinetic current and i_L is Levich current and they are represented as

$$i_K = nFA[\text{substrate}]k_{cat}\Gamma_{cat} \quad (3)$$

and

$$i_L = 0.62nFA[\text{substrate}](D_{substrate})^{2/3}\omega^{1/2}\upsilon^{-1/6} \quad (4)$$

Here, n = number of electrons transferred to the substrate (redox active species like $[Fe(CN)_6]^{3-}$ or cyt *c*), F = Faraday constant, A = macroscopic area of the electrode (for Au disc, A is 0.19625 cm^2), [substrate] = concentration of substrate (here, the redox active species is considered as the substrate) in solution, k_{cat} = second-order rate constant (here, only ET happens from the electrode to the substrate and thus it will signify k_{ET}), Γ_{cat} = catalyst concentration in moles cm^{-2} (in our case the electroactive sites of the Au electrode, either modified or bare acts as catalyst and the surface coverage of the SAM on the Au electrode is equivalent to the catalyst concentration), $D_{substrate}$ = diffusion coefficient of the substrate in the solution, ω = angular velocity of the disc and υ = kinematic viscosity of the solution (0.009 cm^2 s^{-1}).[51] The slope of the linear plot of i^{-1} (inverse of current at various rotation rates) *versus* $\omega^{-1/2}$ (inverse square root of the angular rotation rate) gives the number of electrons involved in the process (eqn (2) and (4)). The second-order rate constant for ET (k_{ET}) occurring from the electrode to the substrate is determined from the intercept of the i^{-1} *versus* $\omega^{-1/2}$ plot (Fig. S2;† eqn (2) and (3)). This second-order ET rate is calculated at several applied potentials between −0.05 V to −0.15 V with a gap of 5 mV in the mass transfer limited region of the current *i.e.*, the plateau current. The determined rate is $\sim 2.51 \pm 0.14 \times 10^5$ M^{-1} s^{-1} at 283 K and the rate increases to $\sim 3.16 \pm 0.15 \times 10^5$ M^{-1} s^{-1}, $\sim 4.56 \pm 0.11 \times 10^5$ M^{-1} s^{-1} and $5.06 \pm 0.22 \times 10^5$ M^{-1} s^{-1} at 288 K, 293 K and 298 K, respectively (Fig. S3†). The diffusion coefficient of $K_3[Fe(CN)_6]$ in 100 mM pH 7 sodium phosphate buffer (containing 100 mM KPF_6 as the supporting electrolyte) was calculated from the plot of i_p *versus* the square root of the scan rate ($\nu^{1/2}$) (Fig. S4†) using the following equation:

$$i_p = 0.4463n_pFAC_{cat}(n_pF\nu D/RT)^{1/2} \quad (5)$$

Here, i_p is the maximum non-catalytic current, A is the area of the electrode, C_{cat}, ν, and D represent the concentration of the redox active species, scan rate and diffusion coefficient, respectively.[52,53] The calculated D_{cat} value at 298 K was found to be 7.52×10^{-6} cm^2 s^{-1} which is in good agreement with the previously determined D_{cat} value of the same.[54] The slope of the K–L plot (i^{-1} *versus* $\omega^{-1/2}$, eqn (4)) at different potentials at the mass transfer limited region corresponds to the theoretical estimate for a 1 e^- slope (Fig. S5†). This is consistent with a 1 e^- transfer by ferricyanide. Thus, the rate obtained from the K–L analysis of the RDE data can be interpreted as the rate of ET from the electrode to $[Fe(CN)_6]^{3-}$ in pH 7 sodium phosphate buffer.

ET rates obtained at different temperatures allows us to determine the value of total reorganization energy (λ_{Total}) of $[Fe(CN)_6]^{3-}$ in solution. The Marcus density-of-states model for ET processes can be used to formulate the Arrhenius plot of $\ln(kT^{-1/2})$ *versus* T^{-1} (eqn (6)).[55,56]

$$\lambda = -4.03\ d(\ln[k_{ET}T^{-1/2}])/d[T^{-1}] \quad (6)$$

Assuming λ_{Total} to be temperature independent, its numerical value is determined from the slope of the plot of $\ln[k_{ET}T^{-1/2}]$ *versus* T^{-1}(Fig. 2A).[55,56] The λ_{Total} obtained at different potentials (Fig. 2B, Fig. S6†) in the mass transfer limited region indicates a value of 1.41 ± 0.04 eV. Since an aqueous solution of $[Fe(CN)_6]^{3-}$ is used, the λ_{Total} determined from the RDE analysis includes both inner-sphere and outer-sphere contributions ($\lambda_{Total} = \lambda_{IS} + \lambda_{OS}$). This value is close to that determined from photoelectron spectroscopic measurements (1.47 eV).[57] These results validate the use of RDE as an experimental tool for the determination of λ_{Total} of a redox active species in solution.

(B) Bovine heart cyt *c* (b-cyt *c*). The λ_{Total} of bovine heart cyt *c* (b-cyt *c*) is determined similarly. Note that the sequence of b-cyt *c* differs from that of the well-studied horse heart cyt *c* at only three residues, T47S, K60G, and T89G, where the last residues correspond to bovine.[58] The b-cyt *c* does not show electrochemical activity with a metal electrode,[59–62] thus the electrode has to be modified.[63–65] An Au electrode modified with 6-mercaptohexanoic acid SAM is used as the working electrode in a pH 6 sodium phosphate buffer solution. Under these conditions the –COOH groups of the SAM are deprotonated,[40] resulting in a negatively charged electrode surface, which should facilitate the interaction between the electrode and b-cyt *c* protein, which has an isoelectric point of 9.6 (ref. 66) and thus an overall positive charge at pH 6.[63,67–69] Indeed, a patch of positively charged residues clustered near the solvent-exposed

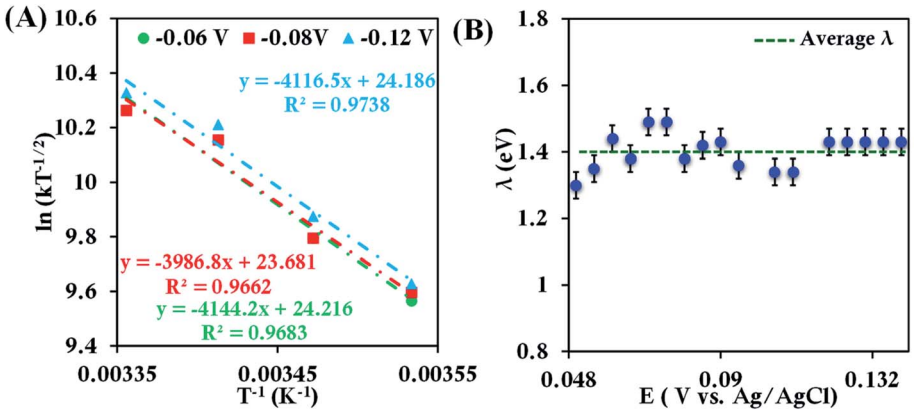

Fig. 2 (A) Arrhenius semilogarithmic plot of $\ln(kT^{-1/2})$ *versus* T^{-1} for 1 mM $K_3[Fe(CN)_6]$ in 100 mM pH 7 sodium phosphate buffer containing 150 mM KPF_6 at three different potentials. From these slopes λ_{Total} values at different potentials were determined. The remaining data are shown in Fig. S6.† (B) Values of λ_{Total} determined at various potentials in the mass transfer limited region of the RDE voltammograms. Here, freshly washed Au disc was used as working electrode, aqueous Ag/AgCl (saturated KCl) and Pt electrodes were used as reference and counter electrode, respectively.

heme edge is proposed to be the site of interaction between b-cyt *c* and redox partners.[17,48] The high ionic strength (150 mM) excludes binding of b-cyt *c* to the electrode,[23] which is confirmed with a rinse test (Fig. S7†) and the linear dependence of faradaic current with the square root of the scan rate in RDE experiments (Fig. S8†).

The native protein structure is preserved upon binding of cyt *c* to the 6-mercaptohexanoic acid SAM modified electrode[70,71] and the protein experiences a strong electric field near the electrode surface.[72–76] Previously, it has been shown that under strong electric field the reorientation of the protein at the electrode surface is restricted and it is the rate-limiting step of the ET event.[70,71,76] Murgida and coworkers have observed kinetic isotope effect (KIE) during ET in the presence of short SAM.[72,77] A KIE value of 1.2 was observed for the C_6 carboxylate SAM (used in our experiment) and the value increases in going to thinner SAMs. But, for the thicker SAMs ($n \geq 11$) no such difference in the ET rate was observed in H_2O and D_2O. The alteration of the hydrogen bonding interactions in the protein and protein/SAM interface were held responsible for this observed KIE under high electric field. In a recent study, a prominent KIE was seen during ET through thiol SAMs modified Au electrode to the covalently attached ferrocene.[78] The value of KIE measured was ~2 for C_8SH modified Au electrode. The rate of H/D exchange is fast in the case of C_8SH in compared to the same in C_{16}SH SAM as the number of defects increases for thinner SAMs. Thus, this interfacial KIE at the Au–thiol interface may be a contributor towards the observed KIE during ET observed by Murgida and co-workers. Due to the presence of strong electric field the dipole moment of the adsorbed protein tends to align more effectively resulting in an average perpendicular orientation of the heme active site plane to the surface of the modified electrode.[71] This orientation may not be the best orientation in terms of efficient ET but the restricted orientation helps us to understand the other factors in thee active site that affect the ET.

The CV of b-cyt *c* (Fig. S8†) with the modified electrode indicates a diffusion-limited current. A plot of i_p *versus* the square root of the scan rate ($\nu^{1/2}$) (Fig. S9†) yields (using eqn (5)) the diffusion coefficient of b-cyt *c* in pH 6 sodium phosphate buffer with 150 mM KPF_6 as 2.9×10^{-6} cm^2 s^{-1}. The value of D_{cat} determined here is in close agreement with the value 1.1×10^{-6} cm^2 s^{-1} previously reported for b-cyt *c*.[79] RDE shows increasing current with an increase in rotation speed (Fig. S10†). With the help of K-L analysis both of the number of e^- involved and the rates of ET are estimated. The surface coverage of 6-mercaptohexanoic acid SAM was determined by reductive desorption method described elsewhere[40] and was calculated to be 4.8×10^{-11} moles cm^{-2} (area under the corresponding cyclic voltammograms shows the concentration of the proteins present at the modified electrodes are nearly same, Table ST1†). The slope of the K–L plot collected over a reasonable potential range between 0.05 V to 0.12 V is close to the value of theoretical 1 e^- slope (Fig. S11†). The second-order rate constant was determined from the intercept of the K–L plot at eleven different potentials from 0.05 V to 0.12 V in the mass transfer limited region of the RDE current (Fig. S12†). The rates were determined to be $5.83 \pm 0.8 \times 10^4$ M^{-1} s^{-1}, $6.42 \pm 0.7 \times 10^4$ M^{-1} s^{-1}, $9.62 \pm 1.4 \times 10^4$ M^{-1} s^{-1}, $1.17 \pm 1.7 \times 10^5$ M^{-1} s^{-1}, $1.25 \pm 0.20 \times 10^5$ M^{-1} s^{-1} and $1.43 \pm 0.20 \times 10^5$ M^{-1} s^{-1} at 283 K, 288 K, 293 K, 298 K, 303 K and 308 K, respectively. Rates at different temperatures allow the estimation of λ_{Total} using an Arrhenius semilogarithmic plot of $\ln(kT^{-1/2})$ *versus* T^{-1} as discussed earlier (Fig. 3). The λ_{Total} is determined to be 1.06 ± 0.05 eV which agrees well with the reported values of reorganization energy of cyt *c* proteins which vary between 0.8 eV and 1.2 eV depending on the redox partner.[1,2,25,50,80–90]

Thus, the λ_{Total} values obtained using K–L analysis of RDE data for two different well-defined redox active species, $[Fe(CN)_6]^{3-}$ and b-cyt *c*, agree well with the values of reorganization energy values reported earlier, which validates the approach used here. This method is now extended to cyt c_{552} from *Hydrogenobacter thermophilus* (HtWT) and two of it's site-

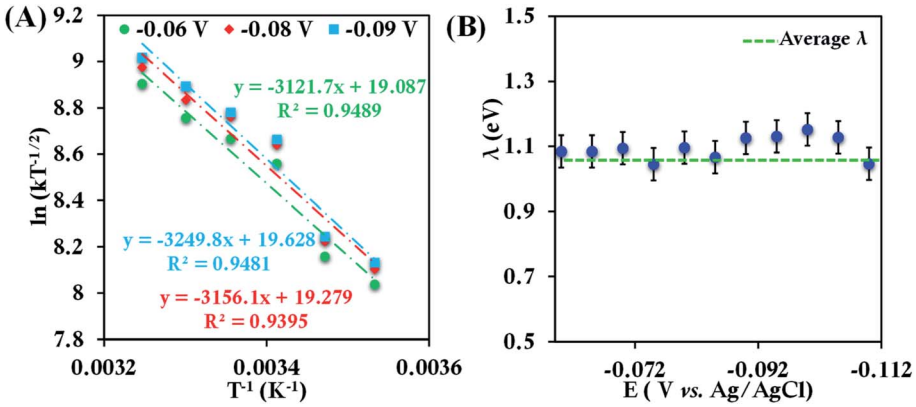

Fig. 3 (A) Arrhenius semilogarithmic plot of $\ln(kT^{-1/2})$ *versus* T^{-1} for 100 μM bovine heart cyt *c* in 100 mM pH 6 sodium phosphate buffer with 150 mM KPF_6 as supporting electrolyte, at three different potentials. From these slopes λ_{Total} was determined. The remaining data are given in Fig. S13.† (B) λ_{Total} values determined at various potentials in the mass transfer limited region of the RDE voltammograms. Here 6-mercapto-hexanoic acid modified Au disc was used as working electrode, aqueous Ag/AgCl (saturated KCl) and Pt electrodes were used as reference and counter electrode respectively.

directed mutants with altered heme axial Met orientations to gain insight into how the heme axial Met orientation and second-sphere interactions at the active site influence the reorganization values in these proteins. Note that, for these mutants, λ_{Total} values were evaluated by calculating the rates at three different temperatures instead of four or six. A different set of data for the determination of λ_{Total} using the rates at three different temperatures (Fig. S14–S18†) matches exactly with the value evaluated with the rates at six different temperature for b-cyt *c*. This comparison is provided in the ESI (Fig. S14–S18).†

(C) HtWT and its mutants. Cyclic voltammograms of HtWT were obtained at three different temperatures (283 K, 298 K and 313 K) using the SAM modified Au electrode in 100 mM pH 6 sodium phosphate buffer with 150 mM KPF_6 as supporting electrolyte (Fig. S19†). The second-order ET rate constant (k_{ET}) for HtWT is calculated from the intercept of the K–L plot obtained using the mass transfer limited region of the corresponding RDE voltammograms (Fig. S20†). The value of k_{ET} (second order) increases from $5.93 \pm 0.32 \times 10^4$ M^{-1} s^{-1} to $18.40 \pm 1.80 \times 10^4$ M^{-1} s^{-1} to $22.90 \pm 1.70 \times 10^4$ M^{-1} s^{-1} at 283 K, 298 K and 313 K, respectively (Fig. S21†). The ET rate varies with temperature and using the approach described above, the λ_{Total} is determined to be 1.36 ± 0.03 eV using data from the mass transfer limited regions of the RDE voltammograms (Fig. 4).

In the case of HtQ64V in 100 mM pH 6 sodium phosphate buffers containing 150 mM KPF_6, the temperature dependent cyclic voltammograms show responses near −0.015 V (Fig. S23†). The second-order ET rate constant determined from RDE (Fig. S24†) is $5.98 \pm 0.52 \times 10^4$ M^{-1} s^{-1} at 298 K, which decreases to $2.88 \pm 0.27 \times 10^4$ M^{-1} s^{-1} at 283 K and increases to $9.73 \pm 0.90 \times 10^4$ M^{-1} s^{-1} at 313 K (Fig. S25†). The RDE data and corresponding K–L plot for HtQ64V obtained at these temperatures were used to obtain the λ_{Total}. The λ_{Total} is

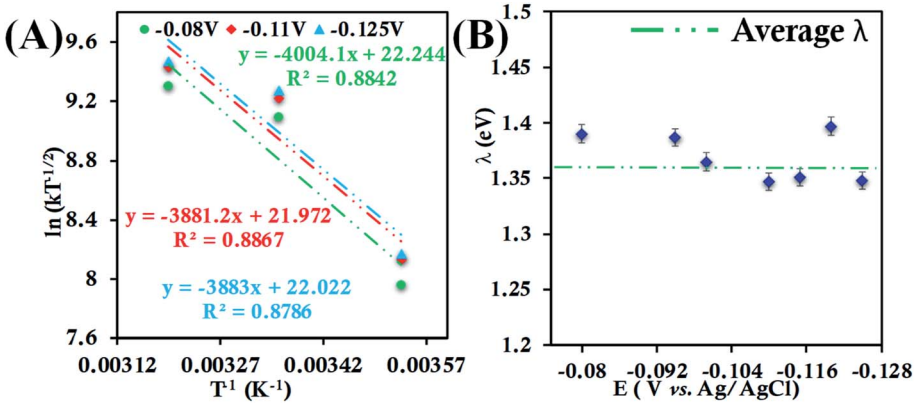

Fig. 4 (A) Arrhenius semilogarithmic plot of $\ln(kT^{-1/2})$ *versus* T^{-1} for 135 μM HtWT in pH 6 sodium phosphate buffer with 150 mM KPF_6 as supporting electrolyte at three different potentials. The remaining data are shown in Fig. S22.† From these slopes λ_{Total} was determined. (B) λ_{Total} values at different potentials determined from the mass transfer limited region of the RDE plots. Here, 6-mercaptohexanoic acid-modified Au disc was used as working electrode, aqueous Ag/AgCl (saturated KCl) and Pt electrodes were used as reference and counter electrode respectively.

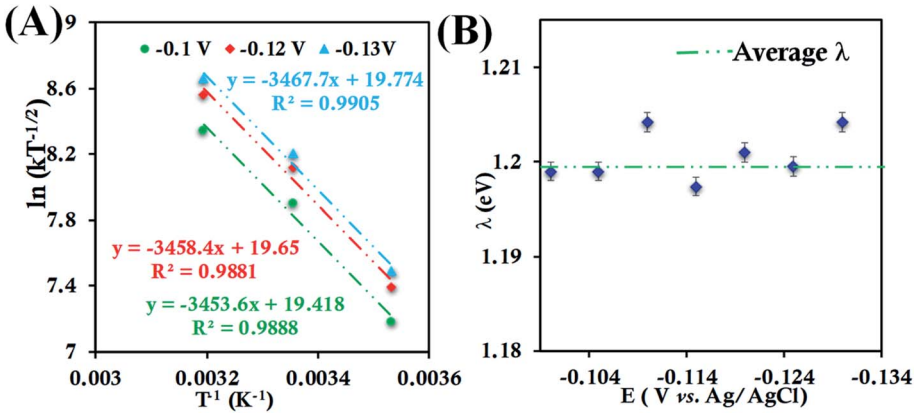

Fig. 5 (A) Arrhenius semilogarithmic plot of $\ln(kT^{-1/2})$ *versus* T^{-1} for 135 μM HtQ64V in 100 mM pH 6 sodium phosphate buffer with 150 mM KPF_6 as supporting electrolyte at three different potentials. The remaining data are shown in Fig. S26.† From these slopes λ_{Total} was determined. (B) λ_{Total} values determined at various potentials in the mass transfer limited region of the RDE plots. Here, 6-mercaptohexanoic acid modified Au disc was used as the working electrode, aqueous Ag/AgCl (saturated KCl) and Pt electrodes were used as reference and counter electrodes, respectively.

determined to be 1.20 ± 0.01 eV across the mass transfer limited potential region (Fig. 5).

Cyclic voltammograms and RDE voltammograms of HtQ64N in 100 mM pH 6 sodium phosphate buffer (150 mM KPF_6) using a 6-mercaptohexanoic acid SAM-modified Au electrode as a working electrode were obtained at different temperatures (Fig. S27, S28A, C and E†). K–L analysis at different temperatures (Fig. S28B, C and D†) yields second-order k_{ET} values of 3.93 ± 0.61 × 10^4 M^{-1} s^{-1} (at 283 K), 9.11 ± 0.80 × 10^4 M^{-1} s^{-1} (at 298 K) and 11.90 ± 1.30 × 10^4 M^{-1} s^{-1} (at 313 K) (Fig. S29†). The λ_{Total} of HtQ64N in 100 mM pH 6 sodium phosphate buffer is determined to be 1.26 ± 0.02 eV using Arrhenius semilogarithmic plot ($\ln kT^{-1/2}$ *versus* T^{-1}) (Fig. 6A) with varying potentials (Fig. 6B).

These values of λ_{Total} for HtWT and two of its mutants determined using an RDE technique are similar to each other and of a magnitude expected based on other determinations of reorganization energies for cytochromes *c*. The values of λ_{Total} differ among the proteins, which may reflect effects of different orientations of the axial methionine and/or the second-sphere residues present in the active site. These relationships are explored further below. Importantly, the reorganization energies obtained using RDE are the λ_{Total} values including both inner-sphere contributions and outer-sphere contributions (consisting of the contributions from both of the protein and the solvent) because the species are freely diffusing in solution. Alternatively, if reorganization energy is determined for proteins immobilized on electrodes, one may expect the outer-sphere contribution to λ, albeit small for a protein like cyt *c*, to decrease because of the displacement of solvent from the protein surface.[6] In the case of these cyt *c* proteins, this would specifically involve the solvent-exposed heme edge through which ET is proposed to occur. This effect can be measured for cyt *c* immobilized on electrodes bearing a negative charge in

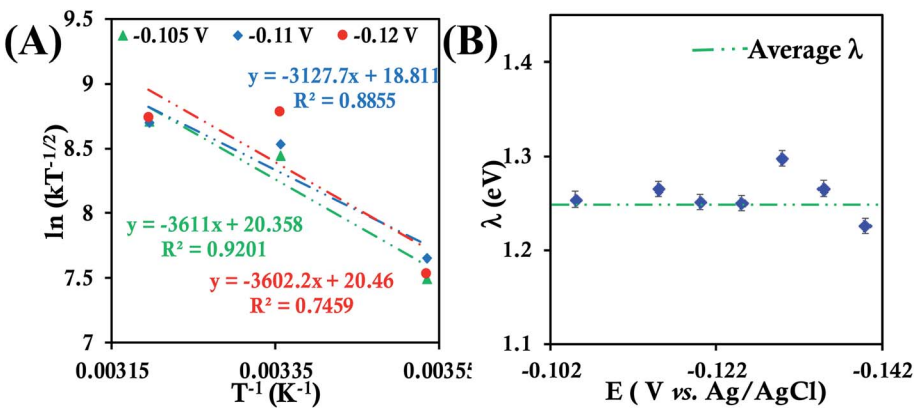

Fig. 6 (A) Arrhenius semilogarithmic plot of $\ln(kT^{-1/2})$ *versus* T^{-1} for 135 μM HtQ64N in 100 mM pH 6 sodium phosphate buffer with 150 mM KPF_6 as supporting electrolyte at three different potentials. The remaining data are shown in Fig. S30.† From these slopes λ_{Total} was determined. (B) λ_{Total} distribution according to various potential in the mass transfer limited region of the RDE plots. Here 6-mercaptohexanoic acid modified Au disc was used as working electrode, aqueous. Ag/AgCl (saturated KCl) and Pt electrodes were used as reference and counter electrode respectively.

solutions at relatively low electrolyte concentration.[23] These results are described in the following sections.

Electron transfer kinetics from chronoamperometry

Here, we determine the apparent heterogeneous electron transfer (ET) rate constant (k_{app}) of redox active species (b-cyt *c*, HtWT, HtQ64V and HtQ64N) by potential step chronoamperometry after attaching the species electrostatically to carboxyl-terminated alkyl thiol self-assembled monolayers modified Au electrode.[39,91] During chronoamperometry, the potential of the electrode is varied from the initial potential, taken as the $E_{1/2}$ of the redox species, to a final potential (E') to drive the oxidation or reduction of the same. At a particular overpotential ($E' - E_{1/2}$) the current follows an exponential relationship with time according to:[39,51]

$$i = k_{app} Q \exp(-k_{app} t) \quad (7)$$

where k_{app} is the apparent electron transfer rate constant and Q is the charge passed during the redox transformation. The current decay observed during chronoamperometry contains two responses, one for the charging current decay and another is faradaic current decay.

(A) Bovine heart cyt *c* (b-cyt c). The cyclic voltammogram of b-cyt *c* in low ionic strength solution (100 mM sodium phosphate, pH 7.3 with 4 mM KPF_6 as supporting electrolyte) collected using a 6-mercaptohexanoic acid-terminated Au electrode at 1 V s^{-1} shows a quasi-reversible response with a $E_{1/2}$ of −68 mV, −62 mV, and −52 mV *versus* Ag/AgCl at 297 K, 287 K, and 279 K, respectively (Fig. S31†). The attachment is electrostatic and can be achieved only at low ionic strength buffer[6] solution and is confirmed with a linear dependence of faradaic current with scan rate[23] (Fig. S32†). Potential step chronoamperometry was performed on b-cyt *c* attached to the modified Au electrode in 100 mM pH 7.3 sodium phosphate buffer with 4 mM KPF_6 as supporting electrolyte (Fig. S33B–D†) and the slope of the corresponding semilogarithmic plot of ln(*i*) *versus* time (Fig. 7) according to eqn (7) yields k_{app} values of 124 ± 9 s^{-1}, 142 ± 12 s^{-1} and 175 ± 17 s^{-1} at 279 K, 287 K and 297 K, respectively, at 50 mV overpotential (both cathodic and anodic overpotential region, Fig. S34†). To avoid the charging current decay completely in the determination of ET rate the linear regression fitting of the ln(*i*) *versus* time plot beyond ~4 milliseconds was considered.[38] The capacitive current decays completely within a 0.6 millisecond time scale (Fig. S33A†). Using Arrhenius analysis of the ET rate at three different

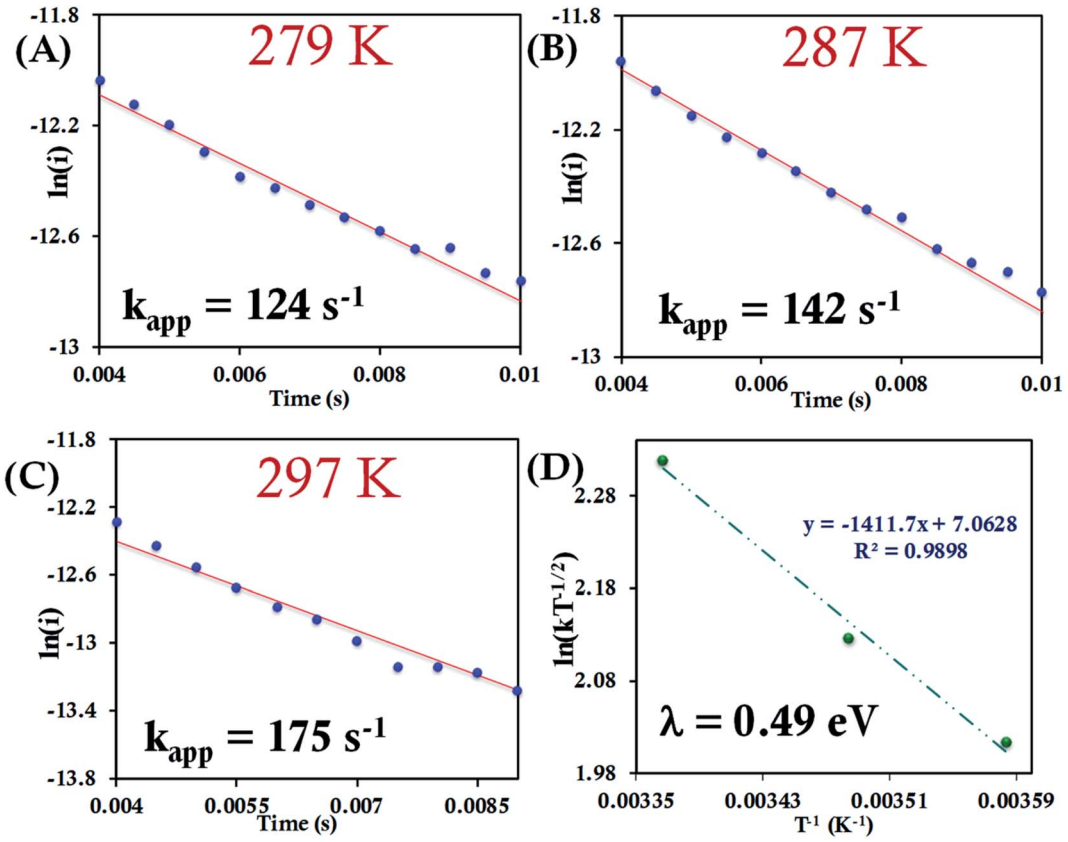

Fig. 7 (A–C) Chronoamperometric semilogarithmic plots for of ln(*i*) *versus* time with regression fittings at different temperatures for b-cyt *c* attached to a 6-mercaptohexanoic acid modified Au electrode. The slope of linear fitting gives the apparent ET rate (eqn (7)). The k_{app} and corresponding temperature are indicated in each graph. The overpotential applied was −50 mV. (D) Arrhenius semilogarithmic plot of $\ln(kT^{-1/2})$ *versus* T^{-1} of the results from panels A, B, C. From the slope λ_{CA} was determined (eqn (6)) as indicated in the graph. Here aqueous Ag/AgCl (saturated KCl) and Pt electrodes were used as reference and counter electrode respectively.

temperatures gives us the value of λ_{CA} as 0.49 ± 0.01 eV (Fig. 7D). Chronoamperometry, performed at higher cathodic overpotential region (−100 mV and −150 mV), yields almost the same value of λ_{CA} (Fig. S35 and S36†). This λ_{CA} value is in good agreement with 0.58 eV, the electrochemically determined reorganization energy value for horse heart cyt *c* attached to ω-hydroxy alkanethiol SAM modified Au electrodes.[6,22] The λ_{CA} value determined by electrochemical methods is highly dependent on the electric field strength.[92] With increasing the chain length of the SAM (decreasing electric field strength) the λ_{CA} value decreases.[25,77,92,93] When the electrode is modified with carboxyl terminated alkyl thiol SAM containing 16 carbon atoms, the reorganization energy value is found to be between 0.26 to 0.35 eV from SERS and electrochemical techniques.[23,25] In the current case, the shorter chain length of the SAM leads to a higher electric field strength and a higher λ_{CA} value. Theoretical calculations have suggested that the λ_{Total} of horse heart cyt *c* is 0.8 eV of which 0.1 eV is λ_{IS}, and the rest is λ_{OS}. Both the protein (0.45 eV) and the solvent (0.25 eV) contribute to the λ_{OS}.[84] For clearer presentation and discussion of the data, we segregate the protein and solvent contributions to λ_{OS} into λ_P and λ_{Solv}, respectively. When the protein is attached electrostatically to a SAM modified electrode, the solvent contribution of λ_{OS} *i.e.* λ_{Solv} is expected to be minimal and the reorganization energy obtained is mostly contributed by λ_{IS} and λ_P. These contributions add up to 0.55 eV which is in very good agreement with 0.49 eV determined here.

(B) HtWT and its mutants. The chronoamperometry data (Fig. S37†) on HtWT electrostatically attached to the modified electrode at different temperatures yield ET rates of 14.7 ± 1.9 s^{-1}, 17.6 ± 1.7 s^{-1}, and 22 ± 1.5 s^{-1} at 283 K, 289 K, and 296 K, respectively (Fig. 8(A–C)). Arrhenius treatment of the temperature-dependent ET rate results in a λ_{CA} of 0.85 ± 0.01 eV (Fig. 8D). Note that a linear dependence of faradaic current with scan rate has also been found for HtWT which indicates that the protein is electrostatically attached to the modified Au electrode. (Fig. S38†).

For the HtQ64V mutant, which has the axial Met fixed in the "*R*" configuration (Fig. 1), the interfacial ET rates were found to be 10.5 ± 1.5 s^{-1}, 12.6 ± 1.1 s^{-1} and 16.0 ± 1.8 s^{-1} 281 K, 286 K and 297 K, respectively (Fig. 9A–C and S39†). An λ_{CA} value of 0.69 ± 0.01 eV was determined for HtQ64V by fitting to eqn (5) as described earlier (Fig. 9D).

The HtQ64N variant has the axial Met in the *S* configuration (Fig. 1). Here, it is found to have a slower interfacial ET rate than HtWT and HtQ64V. The estimated rates are 6.5 ± 0.8 s^{-1}, 7.3 ±

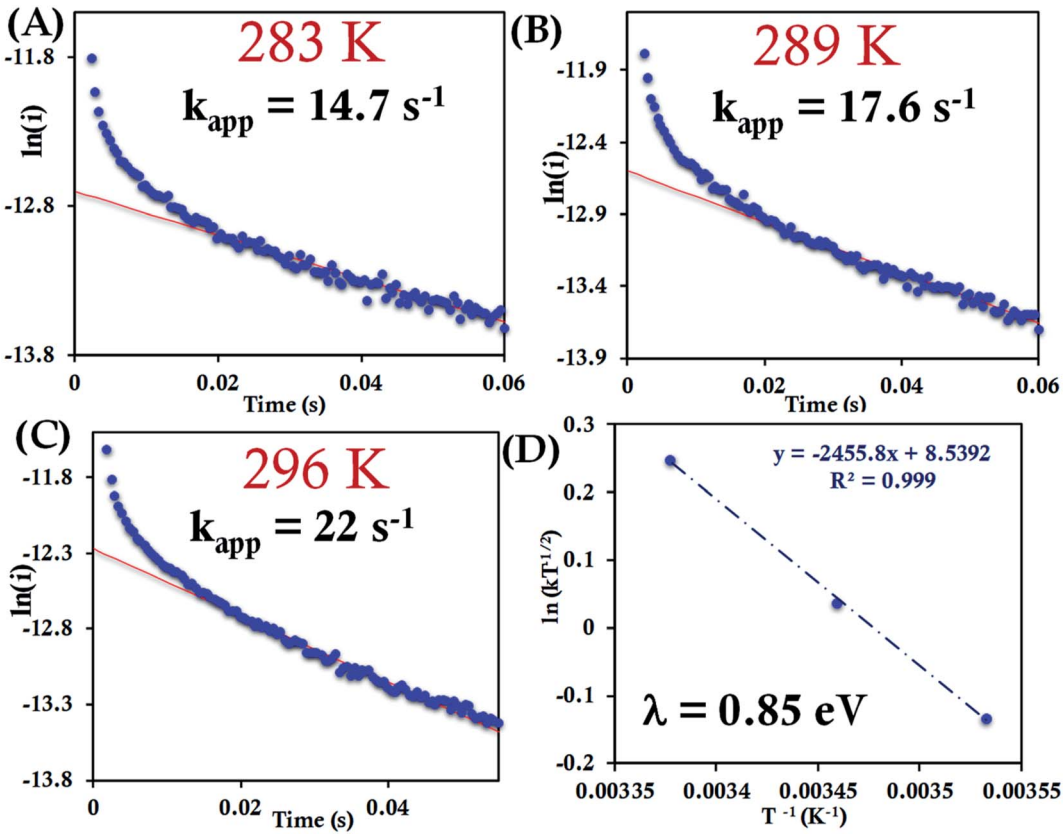

Fig. 8 (A–C) Chronoamperometric semilogarithmic plot of ln(*i*) *versus* time with their regression fittings at different temperature for HtWT attached to 6-mercaptohexanoic acid modified Au wafer. The slope of linear fitting gives the apparent ET rate according to eqn (7). The temperature and k_{app} are indicated in the graph. The overpotential applied was −50 mV. (D) Arrhenius semilogarithmic plot of ln($kT^{-1/2}$) *versus* T^{-1} for HtWT attached to a modified Au wafer in pH 7.3 sodium phosphate buffer (100 mM concentration with 4 mM KPF_6 as supporting electrolyte). From the slopes λ_{CA} was determined as indicated in the graph. Aqueous Ag/AgCl (saturated KCl) and Pt electrodes were used as reference and counter electrode respectively.

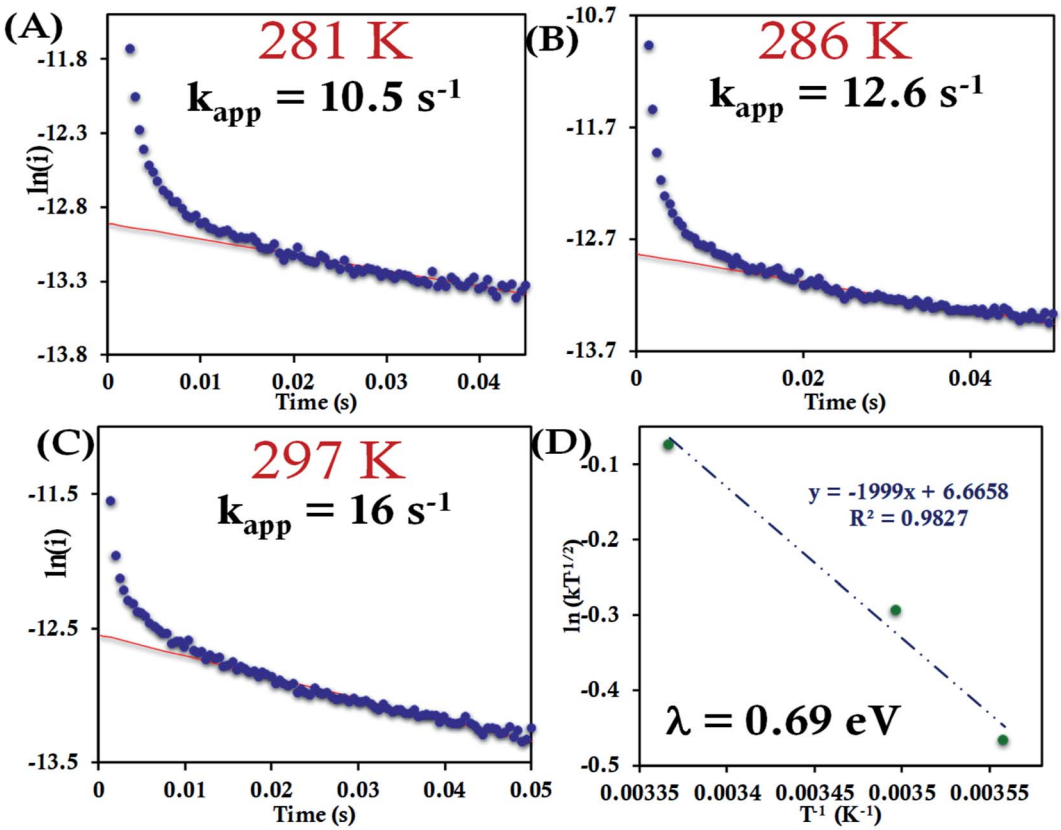

Fig. 9 (A–C) Chronoamperometric semilogarithmic plot of ln(*i*) *versus* time with their regression fittings at different temperature for HtQ64V attached to 6-mercaptohexanoic acid modified Au wafer. The slope of linear fitting gives the apparent ET rate. The temperature and k_{app} are indicated in the graph. The overpotential applied was −50 mV. (D) Arrhenius semilogarithmic plot of ln($kT^{-1/2}$) *versus* T^{-1} for HtQ64V attached to 6-mercaptohexanoic acid terminated Au wafer in 100 mM pH 7.3 sodium phosphate buffer with 4 mM KPF_6 as supporting electrolyte. From the slopes λ was determined as indicated in the graph. Here aqueous Ag/AgCl (saturated KCl) and Pt electrodes were used as reference and counter electrode respectively.

1 s^{-1}, and 9.8 ± 1.2 s^{-1} at 283 K, 287 K, and 297 K, respectively, when attached to the modified Au electrode (Fig. 10A–C, Fig. S40†). The λ_{CA} determined using these values was 0.81 ± 0.02 eV, which falls between the λ_{CA} of HtWT and HtQ64V (Fig. 10D, Table 1).

Electron transfer kinetics from cyclic voltammograms using Laviron's approach

The standard rate constant (k^0) for heterogeneous ET between the electrode and an adsorbed redox active species can be determined by Laviron's method as well.[94] Based upon the Butler–Volmer approach, this method requires sufficient separation between the cathodic and anodic peak potential (ΔE_p > 100 mV) at different scan rates. The resulting transfer coefficient (α) is a measure of the symmetry of the energy barrier of the redox reaction and is generally about 0.5 for the ideal case.[37] However, the value of α may vary depending upon conditions imposed on the redox reaction and consequently determination of α is an important step for the determination of k^0.[37] The anodic and cathodic peak potentials (E_{pa} and E_{pc}, respectively) were plotted separately *versus* ln ν to determine the value of α from the slope using the eqn (8) and (9).

$$E_{PC} = E - (RT/\alpha nF)\ln[\alpha nF/RTk^0] - (RT/\alpha nF)\ln(\nu) \quad (8)$$

$$E_{PA} = E + [RT/(1-\alpha)nF]\ln[(1-\alpha)nF/RTk^0] + [RT/(1-\alpha)nF]\ln(\nu) \quad (9)$$

In these expressions, E_{PA} and E_{PC} are the anodic and cathodic peak potentials, E is the formal potential of the redox-active species (here it is $E_{1/2}$). ν is the scan rate in V s^{-1} and n = 1. Designations of k^0 and α are mentioned above. R, T, n and F have their usual meanings.

At higher scan rates when ΔE_p >100 mV, k^0 was determined from the intercept of the ΔE_p and α value following eqn (10).[37] The details of the approach can be found elsewhere.[15,95]

$$\Delta E_p = 2.3RT/\alpha(1-\alpha)nF[\alpha\log(1-\alpha) + (1-\alpha)\log(\alpha) - \log(RT/nF\nu) - \log(k^0)] \quad (10)$$

For b-cyt *c*, at 297 K a ΔE_p value of 29 mV at 1 V s^{-1} when it is directly attached to the 6-mercaptohexanoic acid terminated Au electrode is obtained, indicating a very fast ET rate, and thus the condition required for applying the Laviron's approach, *i.e.*, ΔE_p > 100 mV can only be obtained at very high scan rates (Fig. S31†). Thus, Laviron's approach is restricted to the

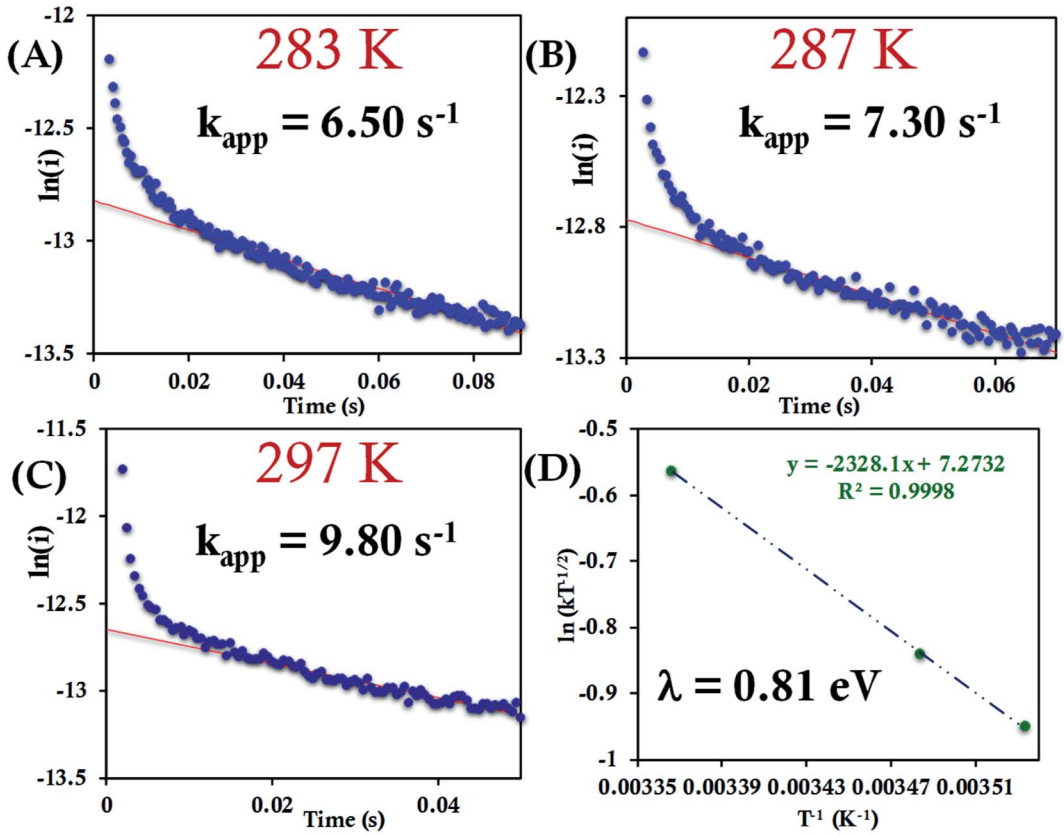

Fig. 10 (A–C) Chronoamperometric semilogarithmic plot of ln(*i*) *versus* time with their regression fittings at different temperature for HtQ64N attached to 6-mercaptohexanoic acid modified Au wafer. The slope of linear fitting gives the apparent ET rate. The temperature and k_{app} were indicated in the graph. The overpotential applied was −50 mV. (D) Arrhenius semilogarithmic plot of ln($kT^{-1/2}$) *versus* T^{-1} for HtQ64N attached to 6-mercaptohexanoic acid modified Au wafer in pH 7.3 phosphate buffer. From the slopes λ_{CA} was determined and indicated in the graph. Here, aqueous Ag/AgCl (saturated KCl) and Pt electrodes were used as reference and counter electrodes, respectively.

determination of ET rate for HtWT cyt *c* and its two mutants, namely HtQ64V and HtQ64N, for which the ΔE_p > 100 mV over a wide range of scan rates.

(A) HtWT cyt *c* and its mutants. The scan rate dependent cyclic voltammogram of HtWT adsorbed to the modified Au electrode is shown in Fig. S41.† From the slope of the linear plot of the cathodic and anodic peak potentials (E_{PA} and E_{PA}, respectively) *versus* ln ν (eqn (8) and (9)), the value of α is estimated to be 0.5, 0.48 and 0.57 at 278 K, 286 K and 296 K, respectively (Fig. S41 and S42†). The slope of the plot of ΔE_p *versus* log ν and the value of α yields the estimated k^0 values of 5.64 ± 0.23 s^{-1}, 7.82 ± 0.35 s^{-1}, and 9.79 ± 0.85 s^{-1} at 278 K, 286 K and 296 K, respectively (Fig. 11A), which in turn allows the estimation of the value of λ_{LV} to be 0.82 ± 0.02 eV using the Arrhenius equation (eqn (5)) as discussed above (Fig. 11B). Notably, the value of λ_{LV} determined using Laviron's approach is very close to the value determined from chronoamperometry (0.85 eV, Table 1, *vide supra*).

In the case of HtQ64V the α values were evaluated as 0.51, 0.40 and 0.56 at 277 K, 282 K, and 298 K, respectively, using the above-defined procedure (Fig. S43 and S44†). The rates were found to be 3.38 ± 0.13 s^{-1}, 4.14 ± 0.18 s^{-1}, and 5.97 ± 0.3 s^{-1} at 277 K, 282 K, 298 K, respectively, and the corresponding λ_{LV} was determined to be 0.71 ± 0.01 eV, again consistent with the chronoamperometric results (0.69 ± 0.01 eV) (Fig. 12).

Determination of the k^0 of HtQ64N attached to the modified Au electrode, using the same approach, yielded rates of 1.17 ± 0.3 s^{-1}, 2.4 ± 0.07 s^{-1} and 3.09 ± 0.08 s^{-1} at 278 K, 283 K and 296 K, respectively (Fig. 13A). The corresponding α is determined to be 0.54, 0.52 and 0.51 at 278 K, 283 K and 296 K, respectively (Fig. S45 and S46†). The value of λ_{LV} estimated using Arrhenius

Table 1 Values of λ determined by various electrochemical methods and their available reported values. λ_{RDE}, λ_{CA}, and λ_{LV} represent determined λ by RDE, chronoamperometry, and Laviron's formalism. λ_{Rep} is the reported λ values as determined by various methods.[1,6,22,25,57,80,81] Note that these reported values are for horse-heart cyt *c*

Species	λ_{Total}[a] (eV)	λ_{CA}[b] (eV)	λ_{LV}[c] (eV)	λ_{Rep}[d] (eV)
$[Fe(CN)_6]^{3-}$	1.41 (±0.04)	—	—	1.47
b-cyt *c*	1.06 (±0.05)	0.49 (±0.01)	—	1.00
HtWT	1.36 (±0.03)	0.85 (±0.01)	0.82 (±0.02)	
HtQ64V	1.20 (±0.01)	0.69 (±0.01)	0.71 (±0.01)	
HtQ64N	1.26 (±0.02)	0.80 (±0.01)	0.80 (±0.01)	

[a] Reorganization energy value measured using RDE. [b] Reorganization energy value measured using Chronoamperometry. [c] Reorganisation energy value measured using CV following Laviron's formalism. [d] Reorganization energy value reported earlier.

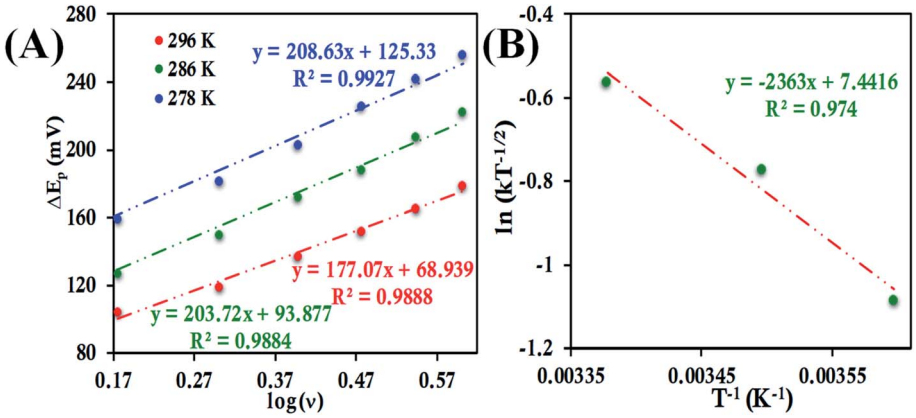

Fig. 11 (A) Plot of ΔE_p *versus* log ν for HtWT attached to 6-mercaptohexanoic acid modified Au wafer at pH 7.3 phosphate buffer at different temperatures. (B) Arrhenius semilogarithmic plot of $\ln(kT^{-1/2})$ *versus* T^{-1} for the same. Here, aqueous Ag/AgCl (saturated KCl) and Pt electrodes were used as reference and counter electrode respectively.

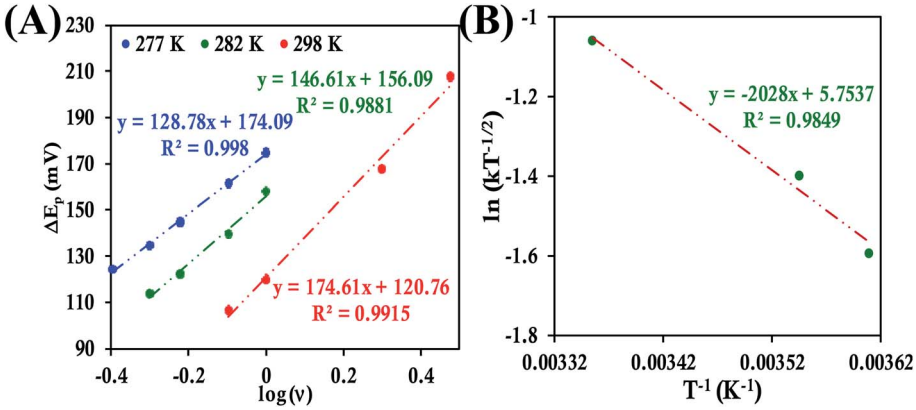

Fig. 12 (A) Plot of ΔE_p *versus* log ν for HtQ64V attached to 6-mercaptohexanoic acid modified Au wafer at pH 7.3 phosphate buffer at different temperatures. (B) Arrhenius semilogarithmic plot of $\ln(kT^{-1/2})$ *versus* T^{-1} for the same. Here, aqueous Ag/AgCl (saturated KCl) and Pt electrodes were used as reference and counter electrode respectively.

analysis was found to be 0.80 ± 0.01 eV using the variable temperature ET rates (Fig. 13B) which is similar to the value obtained from chronoamperometry (also 0.80 ± 0.01 eV).

The experimental values of reorganization energy determined using various electrochemical techniques as well as previously reported values ($[Fe(CN)_6]^{3-}$ and b-cyt *c*) are shown in Table 1. The values of λ, obtained using RDE, are much larger

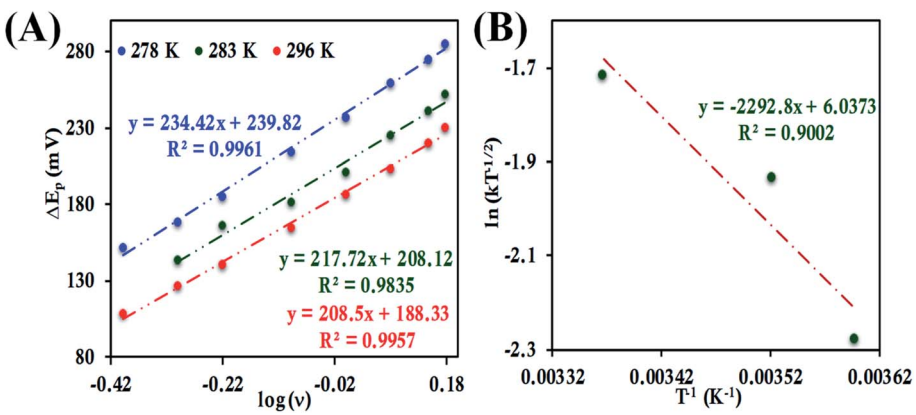

Fig. 13 (A) Plot of ΔE_p *versus* log ν for HtQ64N attached to 6-mercaptohexanoic acid modified Au wafer at pH 7.3 phosphate buffer at different temperatures. (B) Arrhenius semilogarithmic plot of $\ln(kT^{-1/2})$ *versus* T^{-1} for the same. Here, aqueous Ag/AgCl (saturated KCl) and Pt electrodes were used as reference and counter electrode respectively.

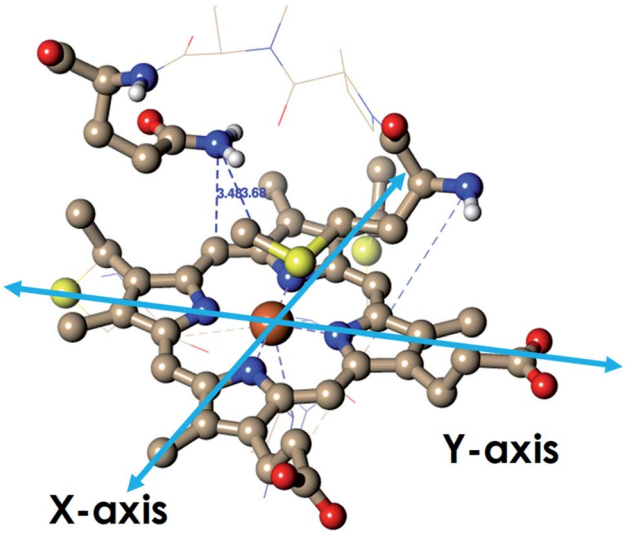

Fig. 14 The active site structure of HtWT where methionine present in *R* conformation used for DFT calculations (PDB ID: 1AYG).

than the values obtained using CA and Laviron's analysis, but the latter two are very similar to each other for each protein. This difference is expected as the RDE technique reports ET parameters from species in solution diffusing to interact with the electrode, while the ET parameters from CA and Laviron's analysis represent those obtained from cyt *c* immobilized on electrodes. It is reasonable to assume that the contribution of λ_{Solv} to λ_{OS} is higher when the protein is in solution relative to the situation when the protein is immobilized on the surface as the λ_{Solv} component to λ_{OS} is reduced. Thus, the difference between the values obtained from RDE (which assesses a diffusing redox species) and CA or Laviron's approach (which assess an immobilized redox species) represents a lower limit of the contribution of λ_{Solv} to λ_{OS}. This assumes that there is minimal structural perturbation of the cyt *c* protein during immobilization.[25] The λ obtained using the CA and Laviron's approaches then represents mostly λ_{IS} and λ_P. In the case of b-cyt *c* this analysis appears to be consistent with previous literature reports on overall λ and $\lambda_{IS} + \lambda_P$ for horse heart cyt *c* (Table 1, column 5) *i.e.*, the λ_{Total} is 1 eV and the $\lambda_{IS} + \lambda_P$ is ~0.5 eV. For HtWT, the λ_{Solv} and $\lambda_{IS} + \lambda_P$ are 0.51 eV and 0.85 eV, respectively, suggesting that the λ_{IS} and λ_P of cyt *c* from Ht is much higher than that of cyt *c* from bovine heart.

Density functional theory (DFT) calculations

Geometry-optimized DFT calculations are used to estimate the λ_{IS} of HtWT and its mutants (Fig. S47†).[14] The axial methionine ligand in the HtWT protein fluctuates between two different conformations; the *R* and the *S* states. In the *R*-state the methionine S–CH_3 bond is oriented along the *Y*-axis (plane containing peripheral $^1CH_3$–$^5CH_3$) of the heme and in the *S*-state it is rotated 90° and is oriented along the *X* axis of the heme (plane containing peripheral $^3CH_3$–$^8CH_3$) (Fig. 14 and 15). The Q64V mutant has the methionine in the *R* state whereas the Q64N mutant has the methionine in the *S*-state.[32,34] The calculated reorganization energy ($\lambda_{cal} = \lambda_{IS}$) for HtWT in the *S*-state and *R*-state are 0.34 eV and 0.31 eV, respectively; this difference reflects the effect of the axial Met configuration only. The λ_{cal} for Q64V (*R*-state) and Q64N (*S*-state) are 0.21 eV and 0.29 eV, respectively. While these variants have different Met configurations, they also have different interactions between residue 64 and the axial Met. While the absolute values of the reorganization energies are lower (using DFT) than the experimentally determined (λ_{CA} or λ_{LV}) values (as only a part of the protein is being modelled computationally, resulting in small contribution of the total λ_P), the difference between them is in very good agreement with the experimental data. For example, the experimentally determined $\lambda_{IS} + \lambda_P$ of the Q64N and the Q64V

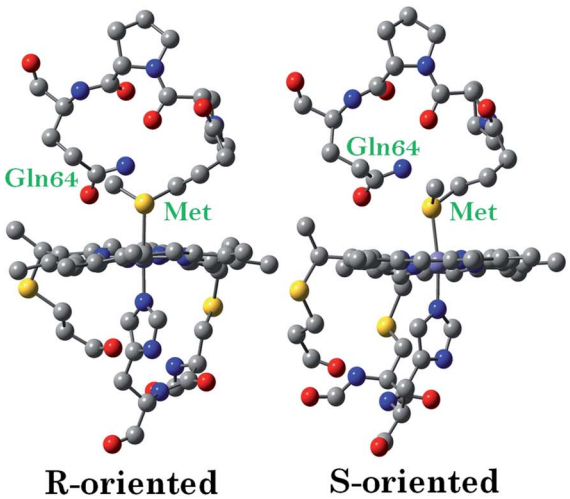

Mutants	λ_{cal} (eV)
HtWT (R-oriented)	0.31
HtWT (S-oriented)	0.34
HtQ64V (R-oriented)	0.21
HtQ64V (S-oriented)	0.24
HtQ64N (R-oriented)	0.23
HtQ64N (S-oriented)	0.29

Fig. 15 The computational model of the HtWT heme pocket used for DFT calculations and the calculated λ_{cal} values of HtWT and two of its mutants with both of *R* and *S* axial Met configurations. Hydrogens are omitted for clarity.

mutants are lower than that of the HtWT by 0.04 eV and 0.16 eV, respectively, whereas the λ_{cal} for the *S*-state of Q64N and *R*-state of Q64V mutants are lower than HtWT (average of *R*-state and *S*-state) λ_{cal} by 0.04 eV and 0.12 eV, respectively. Thus, the factors responsible for the difference in the experimentally estimated value of $\lambda_{IS} + \lambda_P$ are reflected in the computational model as well, *i.e.*, the differences in the λ_P mostly originate from the protein fragment modelled in the DFT calculations.

Computational data indicate that the λ_{cal} of HtWT in its *S*-state is higher than the λ_{cal} of the *R*-state by 0.03 eV. Thus, the rest of the difference seen between these variants (0.09 eV) must be derived from the differences in the changes in geometry of the active site upon change of redox state. The λ_{cal} values are also evaluated by optimizing the geometries using B3LYP functional instead of BP86 and the same trend in the calculated λ values follow (Table ST1†).

The change of geometry upon oxidation is not localized on specific bonds. Rather, it is delocalized over the entire heme ring and results in very small changes for individual C–C and C–N bonds in the heme ring as well as the ligand. However, the change of localization of the hole during the geometric relaxation process can be used to evaluate the extent of geometric change *i.e.*, λ_{IS}. The electron transfer process can be divided into (a) a vertical transition representing the ionization of the HOMO to a Koopmans' state followed by (b) electronic relaxation of the hole created and finally, (c) geometric relaxation (Scheme 1).[96,97]

The HOMO of the ferrous active site is the non-bonding d_{xy} orbital as the d_{xz} and d_{yz} orbitals are stabilized by back bonding to the porphyrin ring π^* orbitals. The energy of the ionization process depends on the energy of the HOMO and in this case (non-bonding HOMO) reflects the Z_{eff} of the metal center. The Koopmans' state relaxes as the hole is allowed to redistribute within the molecule and without any change of geometry. The wavefunction of this state is obtained and the t_2 hole now migrates to a $d_{xz/yz}$ orbital and it stabilized by covalent π donation of the porphyrin ligand. The energy of Koopmans' state for HtWT with *S*-oriented methionine was evaluated to be 6.984 eV, which is the negative ionization energy of the HOMO. The theoretical reduction potential in the gas phase was calculated from the difference of the optimization energy of ferric and ferrous HtWT and found to be 0.75 V. A change in geometry lowers the energy by a further 0.31 eV defined by the reorganization energy of the species. The summation of electronic and geometric relaxation along with the reduction potential reflects the energy of the Koopmans' state. Thus, stabilization by the electronic relaxation is 5.92 eV estimated from the difference. The large electronic relaxation leads to stabilization of the hole created upon oxidation and reduces the need for substantial geometric relaxation, which is key to lowering the λ_{IS} of the ET process. Similarly, large electronic relaxation was observed in Fe_4S_4 proteins which also have very low λ.[98] The change of the ground state wavefunction of the hole

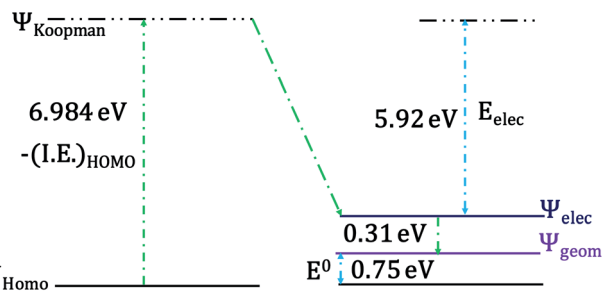

Scheme 1 Schematic diagram of the electronically relaxed and the geometrically relaxed state after vertical ionization of the heme (*S*-oriented methionine). The energy associated with the Koopmans' state, geometric relaxation and electronic relaxation are indicated in the scheme. E^0 is the theoretically determined reduction potential.

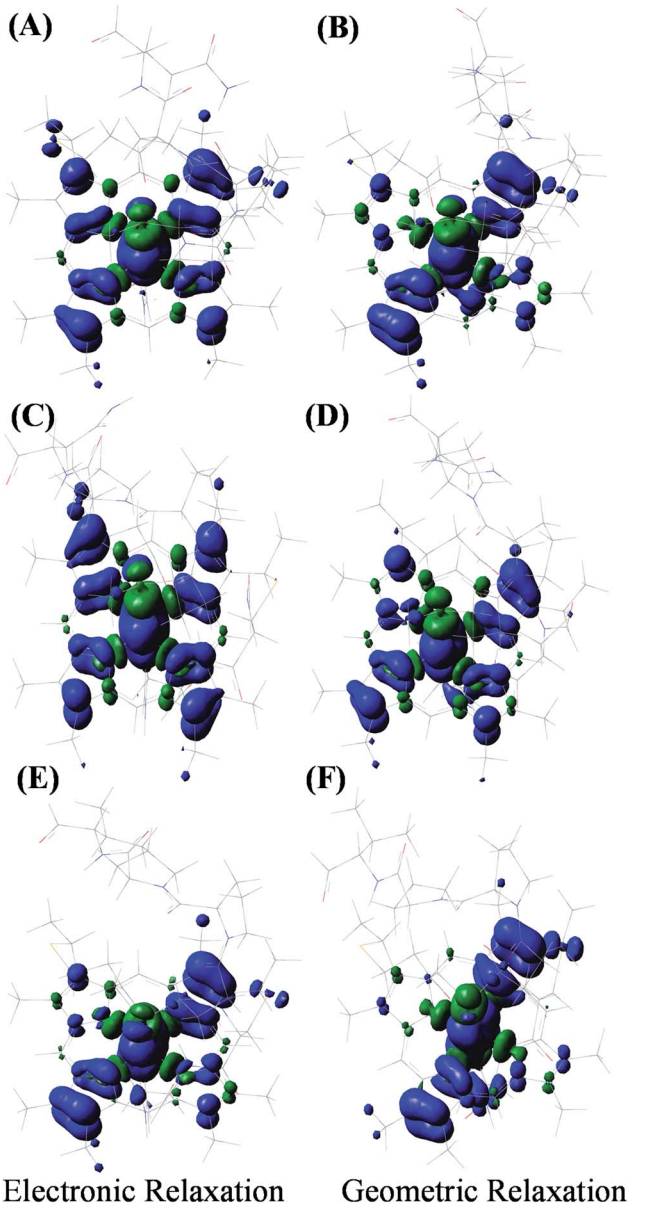

Fig. 16 Spin density distribution of (A and B) HtWT (*S*-conformation form shown), (C and D) Q64N (*S*-conformation), and (E and F) Q64V (*R*-conformation) after immediate oxidation (electronic relaxation) and after the relaxation (geometric relaxation). Blue represents the majority α spin density and green represents β spin density.

created immediately after oxidation (without geometry change) and the final ground state wavefunction of the hole after geometric relaxation indicates a shift of electron density between different parts of the active site, which reflects the small changes of geometry associated with the process. For example, the wavefunction of the t_2 hole in the HtWT model after ionization is more delocalized (on both *Y*-axis and *X*-axis, Fig. 16) than the wavefunction obtained after geometric relaxation where the hole is now localized mainly along the *X*-axis (plane containing peripheral $^{3}CH_3$–$^{8}CH_3$). A substantial change in the extent of delocalization of the hole over the pyrrole rings during the geometric relaxation process automatically implies a higher λ_{cal}. Similarly, the hole created on oxidation of the Q64N mutant in its S-orientation shows re-orientation of the hole during geometric relaxation. Alternatively, the hole created in the case of Q64V mutant is already localized along the *X*-axis and does not change substantially during geometric relaxation, consistent with a smaller calculated λ_{cal}.

Discussion

Here, we demonstrate that the reorganization energies of redox-active species in solution can be determined conveniently using a dynamic electrochemical technique like RDE. The approach treats the electron transfer between the solution species and the electrode surface as an electrocatalytic reaction. The slopes of the K–L plots obtained in these cases agree with the expectations of a $1e^-$ electron transfer reaction. Assuming that the electroactive area of the electrode remains constant with temperature, an Arrhenius-type treatment of the rate obtained at different temperatures allows determination of total reorganization energy (λ_{Total}). The reorganization energy so determined is comprised of both inner-sphere and outer-sphere contributions and the contribution of the electrode surface to λ_{Total} should be minimal.[23] The approach is calibrated with two well-characterized redox systems; $[Fe(CN)_6]^{3-/4-}$ (inorganic complex) and b-cyt *c* (electron transfer protein). The values determined here compare very well with literature values, demonstrating that analysis of RDE data as described herein is a convenient way of determining λ_{Total} of electroactive species in solution. The reorganization energy is also determined for b-cyt *c* attached electrostatically to an electrode using chronoamperometry and cyclic voltammetry (using Laviron's method). The reorganization energy so determined can be expected to have substantially lower outer-sphere contribution from changes in solvation relative to the b-cyt *c* present in solution. Excellent agreement between the value of reorganization energy for the immobilized proteins is observed between these two complementary techniques. Furthermore, the reorganization energy determined using these two methods is almost half of that determined by RDE method for freely diffusing protein, and is very close to past literature reports on reorganization energy of horse-heart cyt c determined by electrochemical methods.[22,30] Thus, within some approximation, the chronoamperometry and Laviron's methods when applied to cyt *c* adsorbed on the modified electrodes reflects the $\lambda_{IS} + \lambda_P$ of the protein (please note that, λ_{Solv} is always present, but its contribution is very small relative to the same for b-cyt c freely diffusing in solution).

These approaches are extended to understand the effect of mutation of the Q64 residue in Ht cyt *c* on reorganization energy and on electron transfer kinetics. The $\lambda_{IS} + \lambda_P$ (λ_{CA}) of HtWT determined from the electrochemical techniques used in this study is ~0.3 eV (Table 1, row 4) more than that of b-cyt *c* determined using the same approach. The estimated $\lambda_{IS} + \lambda_P$ from the electrochemical data on these proteins indicate that the difference in the λ_{Total} is entirely derived from differences in their respective $\lambda_{IS} + \lambda_P$ (Table 1, row 4, 5 and 6). The λ_{Total} values for the Q64V and Q64N mutant are 0.16 eV and 0.10 eV lower than that of HtWT, respectively. Note that these differences between the λ_{Total} in these proteins are well outside of the error of the measurement. The difference in the $\lambda_{IS} + \lambda_P$ of HtWT and HtQ64V is ~0.16–0.12 eV, which suggests that the major contribution to the difference in the λ_{Total} of the two (0.16 eV) seems to originate from the $\lambda_{IS} + \lambda_P$ contribution to λ_{Total}. On the contrary, the $\lambda_{IS} + \lambda_P$ of HtWT and Q64N are very similar, suggesting that the 0.10 eV difference in λ_{Total} is derived from differences in their respective λ_{OS} contribution to λ_{Total}. Notably, NMR analysis of the solution structures of these proteins indicates that the side chain of Q64 is positioned to interact with solvent in HtWT, whereas the N64 side chain in the Q64N variant is buried and interacting with the heme axial Met.[32–34] This structural difference is a possible basis for this difference in outer-sphere reorganization energy.

DFT calculations shed light on the factors that contribute to the differences in $\lambda_{IS} + \lambda_P$ between the HtWT, Q64V and Q64N proteins. The calculated λ_{IS} (λ_{cal}) of the *S*-state is generally 0.02–0.05 eV higher than that of the *R*-state for each variant. The HtWT protein is known to exist in a dynamic equilibrium between the two states in solution at room temperature. Thus, an average of the two λ_{cal} of 0.325 eV is a reasonable approximation. The Q64N mutant resides dominantly in its S-conformation which is computed to have a λ_{cal} of 0.29 eV which is quite close to the average λ_{cal} computed for the HtWT consistent with the experimental data. The Q64V mutant, on the other hand, has a λ_{cal} of 0.21 eV which is about 0.11 eV lower than that of HtWT. This difference has minimal contribution from the methionine orientation (0.02–0.05 eV). Rather, the difference stems from the single mutation of the Q64 residue to V.

The optimized geometry indicates that the Q64 residue is poised over the heme cofactor with short contacts (<3.5 Å). The redox active molecular orbital (RAMO) of HtWT is more delocalized than that of HtQ64V as the RAMO in the later is localized more along the *X*-axis with very minor contribution from the

Table 2 Comparison of H_{AB} determined at room temperature using the rates obtained from the RDE method and corresponding λ values with the help of Marcus equation at 113 mV overpotential

Mutants	H_{AB} (cm^{-1}) η = 113 mV @ 298 K	λ_{Total} (eV)
HtWT	0.84 ± 0.04	1.36 ± 0.03
HtQ64V	0.19 ± 0.01	1.20 ± 0.01
HtQ64N	0.31 ± 0.01	1.26 ± 0.02

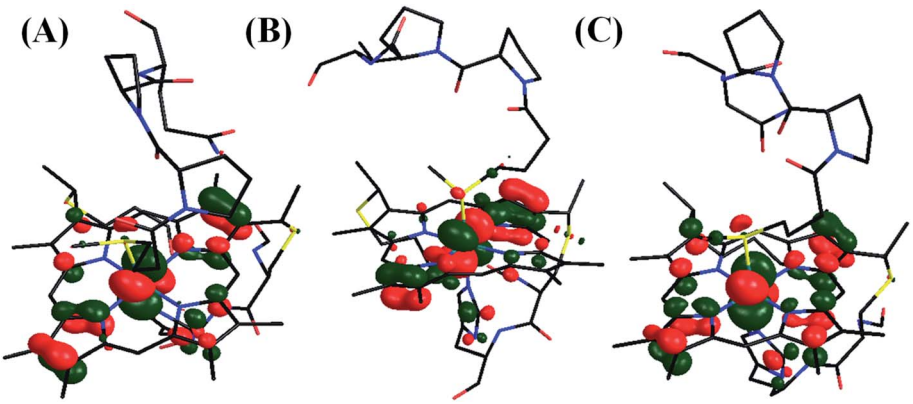

Fig. 17 LUMO of (A) HtWT (modelled here with *S*-oriented methionine), (B) Q64V (*R*-oriented methionine) and (C) Q64N (*S*-oriented methionine) mutant.

pyrroles along the *Y*-axis (Fig. 16E and F). The presence of the glutamine dipole close to the heme polarizes the electron density and directs the partial localization of the hole along the *Y*-axis (Fig. 16A and B). This increases the λ_{cal} of the redox process in the HtWT active site. However, the ET rates of HtWT with greater $\lambda_{IS} + \lambda_P$ are greater than those of the Q64V mutant which has a lower $\lambda_{IS} + \lambda_P$. Thus, the H_{AB} must be enabling faster ET in HtWT despite having higher $\lambda_{IS} + \lambda_P$. Greater delocalization of the RAMO should enhance the electron transfer matrix H_{AB}. Note that in the case the Q64 residue is oriented to the outside of the protein, we propose that water may enter the distal site and have a similar effect. The $^5CH_3$ group along the *Y*-axis is closest to the protein surface and is thus expected to be important for the ET pathway. Thus, having the RAMO delocalized along the *Y*-axis where the $^5CH_3$ is oriented should increase the H_{AB} at the cost of a greater $\lambda_{IS} + \lambda_P$.

In fact, the H_{AB} can be estimated from the ET rates of these proteins and corresponding λ values (Table 2) using the Marcus equation (eqn (1)) with an overpotential (driving force for ET) of 113 mV. The estimated $H_{AB} \sim 1\ cm^{-1}$ represents the ET between the electrode covered SAM and the cyt *c* and the corresponding tunnelling distance is expected to be 13–14 Å based on the Winkler and Gray correlation.[99] This agrees very well with the expected distance of the linker carboxylate thiol from the electrode (Fig. S48†). The estimated H_{AB} for the HtWT is four times greater than that of Q64V mutant. Thus, while the λ_{Total} of the HtWT is ~0.15 eV higher than that of Q64V mutant, the H_{AB} is four times higher. From the Marcus equation (eqn (1)) one can evaluate the relative effect of λ_{Total} and H_{AB} on the ET rate. For simplicity, assuming the driving force for ET to be zero as in self-exchange ET reactions, at room temperature, a ~0.15 eV greater λ_{Total} will reduce the ET rate by a factor of 2.2. However, the rate is more sensitive to H_{AB}, and is expected to increase linearly with the square of H_{AB}. The 4-fold higher H_{AB} in HtWT (Table 2) relative to HtQ64V would result in a 16-fold enhancement in the rate. Thus, although the HtWT has a higher λ_{Total} resulting from the greater polarization of the RAMO, the higher RAMO delocalization in HtWT relative to the two mutants yields a larger H_{AB} and overall, faster self-exchange ET rate (Fig. 17).

Conclusion

In conclusion, we have used dynamic electrochemical techniques for the convenient measurement of the total reorganization energies (λ_{Total}) of redox-active species in solution. The value of reorganization energy thus obtained represents the combination of both the inner-sphere and outer-sphere reorganization energy. This method has been calibrated with two well-characterized redox systems ($[Fe(CN)_6]^{3-}$ and b-cyt *c*). The determined reorganization energy values agree well with previous reports, demonstrating that RDE is a suitable way to determine λ_{Total} of any electroactive species in solution. The reorganization energy is also determined by electrostatically attaching cyt *c* to a modified Au electrode and probing using both chronoamperometry and cyclic voltammetry. These two complementary techniques provide good agreement between the experimentally determined reorganization energy. Values of reorganization energy determined using these techniques are almost half of those determined using the RDE method, consistent with greater contribution of λ_{OS} to the latter and are very close to the previous literature reports. These three electrochemical techniques are then extended to determine the reorganization energy of cyt c_{552} from *Hydrogenobacter thermophilus* (HtWT) (with a fluxional axial methionine (Met) axial ligand) and its two site directed mutants (in which the orientation of the Met group is fixed). We have seen that although HtQ64V shows a lower λ value relative to HtWT, the rate of ET between a modified Au electrode and the protein is greater in the case of HtWT. DFT calculations shed light on the factors contributing to these differences in reorganization energies and in ET rates in these proteins. The RAMO of HtWT is more delocalized than that of HtQ64V, which yields a 4.5-fold increase in the corresponding H_{AB} value for HtWT. This larger H_{AB} value is the key factor responsible for the larger k_{ET} for HtWT despite its greater reorganization energy relative to the HtQ64V mutant. In summary, these results yield detailed insights into contributions of cyt *c* active-site residues to reorganization energy and H_{AB}, key factors controlling ET rates in biology.

Data availability

Additional electrochemical data and optimized coordinates are available in the ESI file.†

Author contributions

A. D. and K. L. B. designed the research. S. C. and M. M. performed the electrochemical experiments. M. M. and B. K. synthesized the HtWT and its mutants. S. C. performed the theoretical calculations. S. C., M. M., A. D. and K. L. B. analyzed the data and S. C., M. M., A. D, and K. L. B. wrote the manuscript. All authors provided feedback on the manuscript.

Conflicts of interest

The authors declare no competing financial interest.

Acknowledgements

This work was supported by the Department of Science and Technology Grant (SERB STR/2019/000081), DST/TMD/HFC/2K18/90(G). S. C. and M. M. acknowledge the IACS IntPCS program.

References

1 H. B. Gray and J. R. Winkler, Electron Transfer in Proteins, *Annu. Rev. Biochem.*, 1996, **65**(1), 537–561.
2 A. Warshel, A. K. Churg and R. Huber, Converting structural changes upon oxidation of cytochrome c to electrostatic reorganization energy, *J. Mol. Biol.*, 1983, **168**(3), 693–697.
3 R. S. Farid, C. C. Moser and P. Leslie Dutton, Electron transfer in proteins, *Curr. Opin. Struct. Biol.*, 1993, **3**(2), 225–233.
4 S. M. Andrew, K. A. Thomasson and S. H. Northrup, Simulation of electron-transfer self-exchange in cytochromes c and b5, *J. Am. Chem. Soc.*, 1993, **115**(13), 5516–5521.
5 J. Liu, S. Chakraborty, P. Hosseinzadeh, Y. Yu, S. Tian, I. Petrik, A. Bhagi and Y. Lu, Metalloproteins Containing Cytochrome, Iron–Sulfur, or Copper Redox Centers, *Chem. Rev.*, 2014, **114**(8), 4366–4469.
6 S. Terrettaz, J. Cheng, C. J. Miller and R. D. Guiles, Kinetic Parameters for Cytochrome c *via* Insulated Electrode Voltammetry, *J. Am. Chem. Soc.*, 1996, **118**(33), 7857–7858.
7 R. H. Holm, P. Kennepohl and E. I. Solomon, Structural and Functional Aspects of Metal Sites in Biology, *Chem. Rev.*, 1996, **96**(7), 2239–2314.
8 H. Shafiey, H. Ghourchian and N. Mogharrab, How does reorganization energy change upon protein unfolding? Monitoring the structural perturbations in the heme cavity of cytochrome c, *Biophys. Chem.*, 2008, **134**(3), 225–231.
9 H. Liu, H. Yamamoto, J. Wei and D. H. Waldeck, Control of the Electron Transfer Rate between Cytochrome c and Gold Electrodes by the Manipulation of the Electrode's Hydrogen Bonding Character, *Langmuir*, 2003, **19**(6), 2378–2387.
10 R. A. Marcus and N. Sutin, Electron transfers in chemistry and biology, *Biochim. Biophys. Acta, Rev. Bioenerg.*, 1985, **811**(3), 265–322.
11 J. R. Winkler, J. Di Bilio Angel, N. A. Farrow, J. H. Richards and H. B. Gray, Electron tunneling in biological molecules, *Pure Appl. Chem.*, 1999, **71**, 1753.
12 X. Amashukeli, N. E. Gruhn, D. L. Lichtenberger, J. R. Winkler and H. B. Gray, Inner-Sphere Electron-Transfer Reorganization Energies of Zinc Porphyrins, *J. Am. Chem. Soc.*, 2004, **126**(47), 15566–15571.
13 R. A. Marcus, Chemical and Electrochemical Electron-Transfer Theory, *Annu. Rev. Phys. Chem.*, 1964, **15**(1), 155–196.
14 E. Sigfridsson, M. H. M. Olsson and U. Ryde, A Comparison of the Inner-Sphere Reorganization Energies of Cytochromes, Iron–Sulfur Clusters, and Blue Copper Proteins, *J. Phys. Chem. B*, 2001, **105**(23), 5546–5552.
15 S. Bandyopadhyay, A. Rana, K. Mittra, S. Samanta, K. Sengupta and A. Dey, Effect of Axial Ligand, Spin State, and Hydrogen Bonding on the Inner-Sphere Reorganization Energies of Functional Models of Cytochrome P450, *Inorg. Chem.*, 2014, **53**(19), 10150–10158.
16 J. I. Blankman, N. Shahzad, B. Dangi, C. J. Miller and R. D. Guiles, Voltammetric Probes of Cytochrome Electroreactivity: The Effect of the Protein Matrix on Outer-Sphere Reorganization Energy and Electronic Coupling Probed through Comparisons with the Behavior of Porphyrin Complexes, *Biochemistry*, 2000, **39**(48), 14799–14805.
17 M. Fedurco, Redox reactions of heme-containing metalloproteins: dynamic effects of self-assembled monolayers on thermodynamics and kinetics of cytochrome c electron-transfer reactions, *Coord. Chem. Rev.*, 2000, **209**(1), 263–331.
18 A. B. Myers, Resonance Raman Intensities and Charge-Transfer Reorganization Energies, *Chem. Rev.*, 1996, **96**(3), 911–926.
19 L. Hu, M. Farrokhnia, J. Heimdal, S. Shleev, L. Rulíšek and U. Ryde, Reorganization Energy for Internal Electron Transfer in Multicopper Oxidases, *J. Phys. Chem. B*, 2011, **115**(45), 13111–13126.
20 K. A. Sharp, Calculation of Electron Transfer Reorganization Energies Using the Finite Difference Poisson-Boltzmann Model, *Biophys. J.*, 1998, **74**(3), 1241–1250.
21 J. E. Frew and H. A. O. Hill, Direct and indirect electron transfer between electrodes and redox proteins, *Eur. J. Biochem.*, 1988, **172**(2), 261–269.
22 J. Cheng, S. Terrettaz, J. I. Blankman, C. J. Miller, B. Dangi and R. D. Guiles, Electrochemical Comparison of Heme Proteins by Insulated Electrode Voltammetry, *Isr. J. Chem.*, 1997, **37**(2–3), 259–266.
23 S. Song, R. A. Clark, E. F. Bowden and M. J. Tarlov, Characterization of cytochrome c/alkanethiolate structures prepared by self-assembly on gold, *J. Phys. Chem.*, 1993, **97**(24), 6564–6572.

24 M. J. Tarlov and E. F. Bowden, Electron-transfer reaction of cytochrome c adsorbed on carboxylic acid terminated alkanethiol monolayer electrodes, *J. Am. Chem. Soc.*, 1991, **113**(5), 1847–1849.

25 D. H. Murgida and P. Hildebrandt, Electrostatic-Field Dependent Activation Energies Modulate Electron Transfer of Cytochrome c, *J. Phys. Chem. B*, 2002, **106**(49), 12814–12819.

26 C. C. Moser, C. C. Page and P. L. Dutton, Darwin at the molecular scale: selection and variance in electron tunnelling proteins including cytochrome c oxidase, *Philos. Trans. R. Soc., B*, 2006, **361**(1472), 1295–1305.

27 G. Basu, A. Kitao, A. Kuki and N. Go, Protein Electron Transfer Reorganization Energy Spectrum from Normal Mode Analysis. 2. Application to Ru-Modified Cytochrome c, *J. Phys. Chem. B*, 1998, **102**(11), 2085–2094.

28 J. Blumberger and G. Lamoureux, Reorganization free energies and quantum corrections for a model electron self-exchange reaction: comparison of polarizable and non-polarizable solvent models, *Mol. Phys.*, 2008, **106**(12–13), 1597–1611.

29 A. K. Churg and A. Warshel, Control of the redox potential of cytochrome and microscopic dielectric effects in proteins, *Biochemistry*, 1986, **25**(7), 1675–1681.

30 I. Muegge, P. X. Qi, A. J. Wand, Z. T. Chu and A. Warshel, The Reorganization Energy of Cytochrome c Revisited, *J. Phys. Chem. B*, 1997, **101**(5), 825–836.

31 D. W. Dixon, X. Hong, S. E. Woehler, A. G. Mauk and B. P. Sishta, Electron-transfer self-exchange kinetics of cytochrome b5, *J. Am. Chem. Soc.*, 1990, **112**(3), 1082–1088.

32 X. Wen and K. L. Bren, Suppression of Axial Methionine Fluxion in Hydrogenobacter thermophilus Gln64Asn Cytochrome c552, *Biochemistry*, 2005, **44**(13), 5225–5233.

33 L. Zhong, X. Wen, T. M. Rabinowitz, B. S. Russell, E. F. Karan and K. L. Bren, Heme axial methionine fluxionality in Hydrogenobacter thermophilus cytochrome c552, *Proc. Natl. Acad. Sci. U. S. A.*, 2004, **101**(23), 8637.

34 M. D. Liptak, X. Wen and K. L. Bren, NMR and DFT Investigation of Heme Ruffling: Functional Implications for Cytochrome c, *J. Am. Chem. Soc.*, 2010, **132**(28), 9753–9763.

35 K. L. Bren, Going with the Electron Flow: Heme Electronic Structure and Electron Transfer in Cytochrome c, *Isr. J. Chem.*, 2016, **56**(9–10), 693–704.

36 R. Kaur and K. L. Bren, Redox State Dependence of Axial Ligand Dynamics in Nitrosomonas europaea Cytochrome c552, *J. Phys. Chem. B*, 2013, **117**(49), 15720–15728.

37 A. L. Eckermann, D. J. Feld, J. A. Shaw and T. J. Meade, Electrochemistry of redox-active self-assembled monolayers, *Coord. Chem. Rev.*, 2010, **254**(15), 1769–1802.

38 R. J. Forster and L. R. Faulkner, Electrochemistry of Spontaneously Adsorbed Monolayers. Equilibrium Properties and Fundamental Electron Transfer Characteristics, *J. Am. Chem. Soc.*, 1994, **116**(12), 5444–5452.

39 H. O. Finklea and D. D. Hanshew, Electron-transfer kinetics in organized thiol monolayers with attached pentaammine(pyridine)ruthenium redox centers, *J. Am. Chem. Soc.*, 1992, **114**(9), 3173–3181.

40 S. Mukherjee, S. Bandyopadhyay and A. Dey, Tuning the apparent formal potential of covalently attached ferrocene using SAM bearing ionizable COOH groups, *Electrochim. Acta*, 2013, **108**, 624–633.

41 R. Meunier-Prest, G. Legay, S. Raveau, N. Chiffot and E. Finot, Potential-assisted deposition of mixed alkanethiol self-assembled monolayers, *Electrochim. Acta*, 2010, **55**(8), 2712–2720.

42 J. Hasegawa, T. Yoshida, T. Yamazaki, Y. Sambongi, Y. Yu, Y. Igarashi, T. Kodama, K.-i. Yamazaki, Y. Kyogoku and Y. Kobayashi, Solution Structure of Thermostable Cytochrome c-552 from Hydrogenobacter thermophilus Determined by 1H-NMR Spectroscopy, *Biochemistry*, 1998, **37**(27), 9641–9649.

43 M. J. Frisch, G. W. Trucks, H. B. Schlegel, G. E. Scuseria, M. A. Robb, J. R. Cheeseman, J. A. Montgomery Jr, T. Vreven, K. N. Kudin, J. C. Burant, J. M. Millam, S. S. Iyengar, J. Tomasi, V. Barone, B. Mennucci, M. Cossi, G. Scalmani, N. Rega, G. A. Petersson, H. Nakatsuji, M. Hada, M. Ehara, K. Toyota, R. Fukuda, J. Hasegawa, M. Ishida, T. Nakajima, Y. Honda, O. Kitao, H. Nakai, M. Klene, X. Li, J. E. Knox, H. P. Hratchian, J. B. Cross, V. Bakken, C. Adamo, J. Jaramillo, R. Gomperts, R. E. Stratmann, O. Yazyev, A. J. Austin, R. Cammi, C. Pomelli, J. W. Ochterski, P. Y. Ayala, K. Morokuma, G. A. Voth, P. Salvador, J. J. Dannenberg, V. G. Zakrzewski, S. Dapprich, A. D. Daniels, M. C. Strain, O. Farkas, D. K. Malick, A. D. Rabuck, K. Raghavachari, J. B. Foresman, J. V. Ortiz, Q. Cui, A. G. Baboul, S. Clifford, J. Cioslowski, B. B. Stefanov, G. Liu, A. Liashenko, P. Piskorz, I. Komaromi, R. L. Martin, D. J. Fox, T. Keith, M. A. Al-Laham, C. Y. Peng, A. Nanayakkara, M. Challacombe, P. M. W. Gill, B. Johnson, W. Chen, M. W. Wong, C. Gonzalez, and J. A. Pople, Gaussian, Inc., Wallingford CT, 2004.

44 R. Krishnan, J. S. Binkley, R. Seeger and J. A. Pople, Self-consistent molecular orbital methods. XX. A basis set for correlated wave functions, *J. Chem. Phys.*, 1980, **72**(1), 650–654.

45 A. D. McLean and G. S. Chandler, Contracted Gaussian basis sets for molecular calculations. I. Second row atoms, Z=11–18, *J. Chem. Phys.*, 1980, **72**(10), 5639–5648.

46 X. Jiang, Z. Futera and J. Blumberger, Ergodicity-Breaking in Thermal Biological Electron Transfer? Cytochrome C Revisited, *J. Phys. Chem. B*, 2019, **123**(35), 7588–7598.

47 X. Jiang, B. Burger, F. Gajdos, C. Bortolotti, Z. Futera, M. Breuer and J. Blumberger, Kinetics of trifurcated electron flow in the decaheme bacterial proteins MtrC and MtrF, *Proc. Natl. Acad. Sci. U. S. A.*, 2019, **116**(9), 3425.

48 C. A. Bortolotti, M. E. Siwko, E. Castellini, A. Ranieri, M. Sola and S. Corni, The Reorganization Energy in Cytochrome c is Controlled by the Accessibility of the Heme to the Solvent, *J. Phys. Chem. Lett.*, 2011, **2**(14), 1761–1765.

49 C. A. Bortolotti, A. Amadei, M. Aschi, M. Borsari, S. Corni, M. Sola and I. Daidone, The Reversible Opening of Water Channels in Cytochrome c Modulates the Heme Iron

Reduction Potential, *J. Am. Chem. Soc.*, 2012, **134**(33), 13670–13678.

50 J. Blumberger, Recent Advances in the Theory and Molecular Simulation of Biological Electron Transfer Reactions, *Chem. Rev.*, 2015, **115**(20), 11191–11238.

51 A. J. Bard and L. R. Faulkner, *Electrochemical Methods: Fundamentals and Applications*. Wiley, 2nd edn, 2000.

52 S. M. Barnett, K. I. Goldberg and J. M. Mayer, A soluble copper–bipyridine water-oxidation electrocatalyst, *Nat. Chem.*, 2012, **4**, 498.

53 W. Schöfberger, F. Faschinger, S. Chattopadhyay, S. Bhakta, B. Mondal, J. A. A. W. Elemans, S. Müllegger, S. Tebi, R. Koch, F. Klappenberger, M. Paszkiewicz, J. V. Barth, E. Rauls, H. Aldahhak, W. G. Schmidt and A. Dey, A Bifunctional Electrocatalyst for Oxygen Evolution and Oxygen Reduction Reactions in Water, *Angew. Chem., Int. Ed.*, 2016, **55**(7), 2350–2355.

54 A. Purwidyantri, C.-H. Chen, L.-Y. Chen, C.-C. Chen, J.-D. Luo, C.-C. Chiou, Y.-C. Tian, C.-Y. Lin, C.-M. Yang, H.-C. Lai and C.-S. Lai, Speckled ZnO Nanograss Electrochemical Sensor for Staphylococcus epidermidis Detection, *J. Electrochem. Soc.*, 2017, **164**(6), B205–B211.

55 J. F. Smalley, S. W. Feldberg, C. E. D. Chidsey, M. R. Linford, M. D. Newton and Y.-P. Liu, The Kinetics of Electron Transfer Through Ferrocene-Terminated Alkanethiol Monolayers on Gold, *J. Phys. Chem.*, 1995, **99**(35), 13141–13149.

56 W.-c. Park and H.-G. Hong, Determination of Reorganization Energy from the Temperature Dependence of Electron Transfer Rate Constant for Hydroquinone-tethered Self-assembled Monolayers (SAMs), *Bull. Korean Chem. Soc.*, 2006, **27**(3), 381–385.

57 R. Seidel, S. Thürmer, J. Moens, P. Geerlings, J. Blumberger and B. Winter, Valence Photoemission Spectra of Aqueous $Fe^{2+}/^{3+}$ and $[Fe(CN)_6]^{4-/3-}$ and Their Interpretation by DFT Calculations, *J. Phys. Chem. B*, 2011, **115**(40), 11671–11677.

58 M. C. Thielges, J. Zimmermann, P. E. Dawson and F. E. Romesberg, The Determinants of Stability and Folding in Evolutionarily Diverged Cytochromes c, *J. Mol. Biol.*, 2009, **388**(1), 159–167.

59 X. Chen, H.-Y. Long, W.-L. Wu and Z.-S. Yang, Direct electrochemical behavior of cytochrome c on sodium dodecyl sulfate modified electrode and its application to nitric oxide biosensor, *Thin Solid Films*, 2009, **517**(8), 2787–2791.

60 Y. Zhou, J. Zhi, Y. Zou, W. Zhang and S.-T. Lee, Direct Electrochemistry and Electrocatalytic Activity of Cytochrome c Covalently Immobilized on a Boron-Doped Nanocrystalline Diamond Electrode, *Anal. Chem.*, 2008, **80**(11), 4141–4146.

61 S. López-Bernabeu, F. Huerta, E. Morallón and F. Montilla, Direct Electron Transfer to Cytochrome c Induced by a Conducting Polymer, *J. Phys. Chem. C*, 2017, **121**(29), 15870–15879.

62 H. Yue and D. H. Waldeck, Understanding interfacial electron transfer to monolayer protein assemblies, *Curr. Opin. Solid State Mater. Sci.*, 2005, **9**(1), 28–36.

63 J. Petrović, R. A. Clark, H. Yue, D. H. Waldeck and E. F. Bowden, Impact of Surface Immobilization and Solution Ionic Strength on the Formal Potential of Immobilized Cytochrome c, *Langmuir*, 2005, **21**(14), 6308–6316.

64 H. Yue, D. Khoshtariya, D. H. Waldeck, J. Grochol, P. Hildebrandt and D. H. Murgida, On the Electron Transfer Mechanism Between Cytochrome c and Metal Electrodes. Evidence for Dynamic Control at Short Distances, *J. Phys. Chem. B*, 2006, **110**(40), 19906–19913.

65 J. Wei, H. Liu, A. R. Dick, H. Yamamoto, Y. He and D. H. Waldeck, Direct Wiring of Cytochrome c's Heme Unit to an Electrode: Electrochemical Studies, *J. Am. Chem. Soc.*, 2002, **124**(32), 9591–9599.

66 M. Graf, R. G. García and H. Wätzig, Protein adsorption in fused-silica and polyacrylamide-coated capillaries, *Electrophoresis*, 2005, **26**(12), 2409–2417.

67 J. J. Wendoloski, J. B. Matthew, P. C. Weber and F. R. Salemme, Molecular dynamics of a cytochrome c-cytochrome b5 electron transfer complex, *Science*, 1987, **238**(4828), 794.

68 M. R. Mauk, A. G. Mauk, P. C. Weber and J. B. Matthew, Electrostatic analysis of the interaction of cytochrome c with native and dimethyl ester heme-substituted cytochrome b5, *Biochemistry*, 1986, **25**(22), 7085–7091.

69 T. L. Poulos and J. Kraut, A hypothetical model of the cytochrome c peroxidase . cytochrome c electron transfer complex, *J. Biol. Chem.*, 1980, **255**(21), 10322–10330.

70 D. A. Paggi, D. F. Martín, A. Kranich, P. Hildebrandt, M. A. Martí and D. H. Murgida, Computer simulation and SERR detection of cytochrome c dynamics at SAM-coated electrodes, *Electrochim. Acta*, 2009, **54**(22), 4963–4970.

71 A. Kranich, H. K. Ly, P. Hildebrandt and D. H. Murgida, Direct Observation of the Gating Step in Protein Electron Transfer: Electric-Field-Controlled Protein Dynamics, *J. Am. Chem. Soc.*, 2008, **130**(30), 9844–9848.

72 D. H. Murgida and P. Hildebrandt, Electron-Transfer Processes of Cytochrome c at Interfaces. New Insights by Surface-Enhanced Resonance Raman Spectroscopy, *Acc. Chem. Res.*, 2004, **37**(11), 854–861.

73 D. H. Murgida and P. Hildebrandt, Heterogeneous Electron Transfer of Cytochrome c on Coated Silver Electrodes. Electric Field Effects on Structure and Redox Potential, *J. Phys. Chem. B*, 2001, **105**(8), 1578–1586.

74 C. P. Smith and H. S. White, Theory of the interfacial potential distribution and reversible voltammetric response of electrodes coated with electroactive molecular films, *Anal. Chem.*, 1992, **64**(20), 2398–2405.

75 H. Wackerbarth and P. Hildebrandt, Redox and Conformational Equilibria and Dynamics of Cytochrome c at High Electric Fields, *ChemPhysChem*, 2003, **4**(7), 714–724.

76 J. Wei, H. Liu, D. E. Khoshtariya, H. Yamamoto, A. Dick and D. H. Waldeck, Electron-Transfer Dynamics of Cytochrome C: A Change in the Reaction Mechanism with Distance, *Angew. Chem., Int. Ed.*, 2002, **41**(24), 4700–4703.

77 D. H. Murgida and P. Hildebrandt, Proton-Coupled Electron Transfer of Cytochrome c, *J. Am. Chem. Soc.*, 2001, **123**(17), 4062–4068.

78 S. Chattopadhyay, S. Bandyopadhyay and A. Dey, Kinetic Isotope Effects on Electron Transfer Across Self-Assembled Monolayers on Gold, *Inorg. Chem.*, 2021, **60**(2), 597–605.
79 M. E. Young, P. A. Carroad and R. L. Bell, Estimation of diffusion coefficients of proteins, *Biotechnol. Bioeng.*, 1980, **22**(5), 947–955.
80 K. C. Cho, K. M. Ng, C. L. Choy and C. M. Che, Electron transfer between cytochrome c and metalloporphyrins at high exothermicities, *Chem. Phys. Lett.*, 1986, **129**(5), 521–525.
81 E. Cheung, K. Taylor, J. A. Kornblatt, A. M. English, G. McLendon and J. R. Miller, Direct measurements of intramolecular electron transfer rates between cytochrome c and cytochrome c peroxidase: effects of exothermicity and primary sequence on rate, *Proc. Natl. Acad. Sci. U. S. A.*, 1986, **83**(5), 1330.
82 G. McLendon, Long-distance electron transfer in proteins and model systems, *Acc. Chem. Res.*, 1988, **21**(4), 160–167.
83 D. G. Nocera, J. R. Winkler, K. M. Yocom, E. Bordignon and H. B. Gray, Kinetics of intermolecular and intramolecular electron transfer from ruthenium(II) complexes to ferricytochrome c, *J. Am. Chem. Soc.*, 1984, **106**(18), 5145–5150.
84 D. E. Khoshtariya, J. Wei, H. Liu, H. Yue and D. H. Waldeck, Charge-Transfer Mechanism for Cytochrome c Adsorbed on Nanometer Thick Films. Distinguishing Frictional Control from Conformational Gating, *J. Am. Chem. Soc.*, 2003, **125**(25), 7704–7714.
85 A. K. Churg, R. M. Weiss, A. Warshel and T. Takano, On the action of cytochrome c: correlating geometry changes upon oxidation with activation energies of electron transfer, *J. Phys. Chem.*, 1983, **87**(10), 1683–1694.
86 T. J. Meade, H. B. Gray and J. R. Winkler, Driving-force effects on the rate of long-range electron transfer in ruthenium-modified cytochrome c, *J. Am. Chem. Soc.*, 1989, **111**(12), 4353–4356.
87 J. S. Zhou and M. A. J. Rodgers, Driving force dependence of rate constants of electron transfer within cytochrome c and uroporphyrin complexes, *J. Am. Chem. Soc.*, 1991, **113**(20), 7728–7734.
88 A. J. Di Bilio, M. G. Hill, N. Bonander, B. G. Karlsson, R. M. Villahermosa, B. G. Malmström, J. R. Winkler and H. B. Gray, Reorganization Energy of Blue Copper: Effects of Temperature and Driving Force on the Rates of Electron Transfer in Ruthenium- and Osmium-Modified Azurins, *J. Am. Chem. Soc.*, 1997, **119**(41), 9921–9922.
89 M. Dinpajooh, D. R. Martin and D. V. Matyushov, Polarizability of the active site of cytochrome c reduces the activation barrier for electron transfer, *Sci. Rep.*, 2016, **6**(1), 28152.
90 T. M. Saccucci and J. F. Rusling, Modeling Square-Wave Voltammetry of Thin Protein Films Using Marcus Theory, *J. Phys. Chem. B*, 2001, **105**(26), 6142–6147.
91 C. E. D. Chidsey, Free Energy and Temperature Dependence of Electron Transfer at the Metal-Electrolyte Interface, *Science*, 1991, **251**(4996), 919.
92 H. Khoa Ly, N. Wisitruangsakul, M. Sezer, J.-J. Feng, A. Kranich, I. M. Weidinger, I. Zebger, D. H. Murgida and P. Hildebrandt, Electric-field effects on the interfacial electron transfer and protein dynamics of cytochrome c, *J. Electroanal. Chem.*, 2011, **660**(2), 367–376.
93 H. Khoa Ly, M. Sezer, N. Wisitruangsakul, J.-J. Feng, A. Kranich, D. Millo, I. M. Weidinger, I. Zebger, D. H. Murgida and P. Hildebrandt, Surface-enhanced vibrational spectroscopy for probing transient interactions of proteins with biomimetic interfaces: electric field effects on structure, dynamics and function of cytochrome c, *FEBS J.*, 2011, **278**(9), 1382–1390.
94 E. Laviron, General expression of the linear potential sweep voltammogram in the case of diffusionless electrochemical systems, *J. Electroanal. Chem. Interfacial Electrochem.*, 1979, **101**(1), 19–28.
95 S. D. Mhaske, M. Ray and S. Mazumdar, Covalent linkage of CYP101 with the electrode enhances the electrocatalytic activity of the enzyme: Vectorial electron transport from the electrode, *Inorg. Chim. Acta*, 2010, **363**(12), 2804–2811.
96 P. Kennepohl and E. I. Solomon, Electronic Structure Contributions to Electron-Transfer Reactivity in Iron–Sulfur Active Sites: 1. Photoelectron Spectroscopic Determination of Electronic Relaxation, *Inorg. Chem.*, 2003, **42**(3), 679–688.
97 P. Kennepohl and E. I. Solomon, Electronic Structure Contributions to Electron-Transfer Reactivity in Iron–Sulfur Active Sites: 2. Reduction Potentials, *Inorg. Chem.*, 2003, **42**(3), 689–695.
98 A. Dey, T. Glaser, M. M. J. Couture, L. D. Eltis, R. H. Holm, B. Hedman, K. O. Hodgson and E. I. Solomon, Ligand K-Edge X-ray Absorption Spectroscopy of $[Fe_4S_4]^{1+,2+,3+}$ Clusters: Changes in Bonding and Electronic Relaxation upon Redox, *J. Am. Chem. Soc.*, 2004, **126**(26), 8320–8328.
99 J. R. Winkler and H. B. Gray, Electron Flow through Metalloproteins, *Chem. Rev.*, 2014, **114**(7), 3369–3380.